Inorganic Chemistry
Article

Inorg. Chem. **2010**, *49*, 5897–5911 **5897**
DOI: 10.1021/ic100349d

Dinuclear Cadmium(II), Zinc(II), and Manganese(II), Trinuclear Nickel(II), and Pentanuclear Copper(II) Complexes with Novel Macrocyclic and Acyclic Schiff-Base Ligands Having Enantiopure or Racemic Camphoric Diamine Components

Jue-Chao Jiang, Zhao-Lian Chu, Wei Huang,* Gang Wang, and Xiao-Zeng You

State Key Laboratory of Coordination Chemistry, Nanjing National Laboratory of Microstructures, School of Chemistry and Chemical Engineering, Nanjing University, Nanjing 210093, People's Republic of China

Received February 22, 2010

Four novel [3 + 3] Schiff-base macrocyclic ligands **I**−**IV** condensed from 2,6-diformyl-4-substituted phenols (R = CH_3 or Cl) and enantiopure or racemic camphoric diamines have been synthesized and characterized. Metal-ion complexations of these enantiopure and racemic [3 + 3] macrocyclic ligands with different cadmium(II), zinc(II), manganese(II), nickel(II), and copper(II) salts lead to the cleavage of Schiff-base C═N double bonds and subsequent ring contraction of the macrocyclic ligands due to the size effects and the spatial restrictions of the coordination geometry of the central metals, the steric hindrance of ligands, and the counterions used. As a result, five [2 + 2] and one [1+2] dinuclear cadmium(II) complexes (**1**−**6**), two [2 + 2] dinuclear zinc(II) (**7** and **8**), and two [2 + 2] dinuclear manganese(II) (**9** and **10**) complexes together with one [1+1] trinuclear nickel(II) complex (**11**) and one [1+2] pentanuclear copper(II) complex (**12**), bearing enantiopure or racemic ligands, different substituent groups in the phenyl rings, and different anionic ligands (Cl^-, Br^-, OAc^-, and SCN^-), have been obtained in which the chiral carbon atoms in the camphoric backbones are arranged in different ways (*RRSS* for the enantiopure ligands in **1**, **2**, **4**, **5**, and **7**−**10** and *RSRS* for the racemic ligands in **3**, **6**, **11**, and **12**). The steric hindrance effects of the methyl group bonded to one of the chiral carbon atoms of camphoric diamine units are believed to play important roles in the formation of the acyclic [1 + 1] trinuclear complex **11** and [1 + 2] dinuclear and pentanuclear complexes **6** and **12**. In dinuclear cadmium(II), zinc(II), and manganese(II) complexes **1**−**10**, the sequence of separations between the metal centers is consistent with that of the ionic radii shortened from cadmium(II) to manganese(II) to zinc(II) ions. Furthermore, UV−vis, circular dichroism, ^{1}H NMR, and fluorescence spectra have been used to characterize and compare the structural differences between related compounds.

1. Introduction

The design and synthesis of macrocyclic ligands and their metal−organic coordination compounds are fascinating areas of research, owing to their important chemical, physical, and mechanical properties.[1−3] Macrocyclic Schiff bases are of great importance for their ability to selectively chelate certain metal ions depending on the number, type, and position of their donor atoms, the ionic radius of the metal centers, and the coordination property of the counterions.[4−10] Recently, more and more attention has been paid to the investigation of chiral Schiff-base macrocyclic and acyclic systems because their related chiral complexes bearing specific stereogenic conformation and structural rigidity have found many applications in the field of asymmetric synthesis, molecular recognition, chiral separation, and so on.[11−14] For instance, Ou et al. have reported an example of spontaneous resolution where a racemic nickel(II) complex can be separated by reaction with D- and L-phenylalanine in a mixture of acetonitrile and water,[15] and Gregoliński et al. have demonstrated

*To whom correspondence should be addressed. E-mail: whuang@nju.edu.cn.

(1) Lehn, J. M. *Supramolecular Chemistry: Concepts and Perspectives*; VCH: New York, 1995.
(2) Erxleben, A. *Coord. Chem. Rev.* **2003**, *246*, 203–228.
(3) Atkins, A. J.; Black, D.; Finn, R. L.; Marin-Becerra, A.; Blake, A. J.; Ruiz-Ramirez, L.; Li, W. S.; Schröder, M. *Dalton Trans.* **2003**, 1730–1737.
(4) Bradshaw, J. S.; Krakowiak, K. E.; Izatt, R. M. *Aza-Crown Macrocycles*; Wiley: New York, 1993.
(5) Busch, D. H.; Vance, A. L.; Kolchinski, A. G. *Comprehensive Supramolecular Chemistry*; Pergamon: New York, 1996; Vol. *9*, pp 1−42.
(6) Brooker, S. *Coord. Chem. Rev.* **2001**, *222*, 33–56.
(7) Amendola, V.; Fabbrizzi, L.; Mangano, C.; Pallavicini, P.; Poggi, A.; Taglietti, A. *Coord. Chem. Rev.* **2001**, *219*, 821–837.
(8) Vigato, P. A.; Tamburini, S. *Coord. Chem. Rev.* **2004**, *248*, 1717–2128.
(9) Huang, W.; Zhu, H. B.; Gou, S. H. *Coord. Chem. Rev.* **2006**, *250*, 414–423.
(10) Golcu, A.; Tumer, M.; Demirelli, H.; Wheatley, R. A. *Inorg. Chim. Acta* **2005**, *358*, 1785–1797.
(11) (a) Gao, J.; Reibenspies, J. H.; Martell, A. E. *Angew. Chem., Int. Ed.* **2003**, *42*, 6008–6012. (b) Lukin, O.; Vögtle, F. *Angew. Chem., Int. Ed.* **2005**, *44*, 1456–1477. (c) Gregoliński, J.; Lisowski, J. *Angew. Chem., Int. Ed.* **2006**, *45*, 6122–6126.
(12) Radecka-Paryzek, W.; Patroniak, V.; Lisowski, J. *Coord. Chem. Rev.* **2005**, *249*, 2156–2175.
(13) (a) Ema, T.; Tanida, D.; Sakai, T. *J. Am. Chem. Soc.* **2007**, *129*, 10591–10596. (b) Mahlert, C.; Kopp, F.; Thirlway, J.; Micklefield, J.; Marahiel, M. A. *J. Am. Chem. Soc.* **2007**, *129*, 12011–12018.
(14) Gasser, G.; Belousoff, M. J.; Bond, A. M.; Kosowski, Z.; Spiccia, L. *Inorg. Chem.* **2007**, *46*, 1665–1674.
(15) Ou, G. C.; Jiang, L.; Feng, X. L.; Lu, T. B. *Inorg. Chem.* **2008**, *47*, 2710–2718.

Published on Web 06/01/2010

that the formation and inversion of helicity can be achieved by means of certain lanthanide(III) ion complexations with a chiral nonaazamacrocycle.[16]

Template synthetic approaches have been widely used to prepare macrocyclic ligands and their metal complexes in high yields, where a variety of metal ions can be used as template agents.[3,8,16] In our previous work, quite a number of achiral polyamines have been used to react with 2,6-diformyl-4-substituted phenols via Schiff-base cyclocondensation by sodium(I) template methods to prepare Robson-type macrocyclic ligands and their metal complexes.[17] Recently, chiral (1*R*,2*R*)- and (1*S*,2*S*)- and racemic *trans*-cyclohexane-1,2-diamines have been used to synthesize [3 + 3] macrocyclic Schiff-base ligands, and a series of macrocyclic and acyclic transition-metal complexes have been yielded, accompanied by cleavage of the Schiff-base C=N double bond and rearrangement of the macrocyclic backbone.[8,18,19] However, the conformational inversion of two neighboring chiral centers of *trans*-cyclohexane-1,2-diamines often takes place because of their structural flexibility.

To extend our studies on chiral macrocyclic complexes and avoid inversion of the absolute configuration of *trans*-cyclohexane-1,2-diamines, more rigid 1,3-diamines [D-(+)- and D,L-camphoric diamines with two chiral carbon atoms in their backbones, which are also known as 1,2,2-trimethylcyclopentane-1,3-diamine][20] are first used to prepare enantiopure and racemic Robson-type macrocyclic compounds. By comparing the results before and after the metal-ion complexation, we also found cleavage and rearrangement of the Schiff-base macrocyclic ligands due to scission of the C=N double bond. Herein, we focus on the syntheses and structural and spectral characterizations of [3 + 3] Schiff-base macrocyclic ligands having enantiopure or racemic camphoric diamine components and their series of transition-metal complexes, i.e., five [2+2] dinuclear cadmium(II), one [1 + 2] dinuclear cadmium(II), two [2 + 2] dinuclear zinc(II), two [2 + 2] dinuclear manganese(II), one [1 + 1] trinuclear nickel(II), and one [1 + 2] pentanuclear copper(II) complexes, where detailed comparisons are involved for the manner of arrangements for the chiral carbon atoms in enantiopure and racemic camphoric diamine units and the use of different counterions, apical ligands, and substituted groups.

Scheme 1. Schematic Illustration of the Preparation of [3 + 3] Macrocyclic Ligands **I**−**IV**[a]

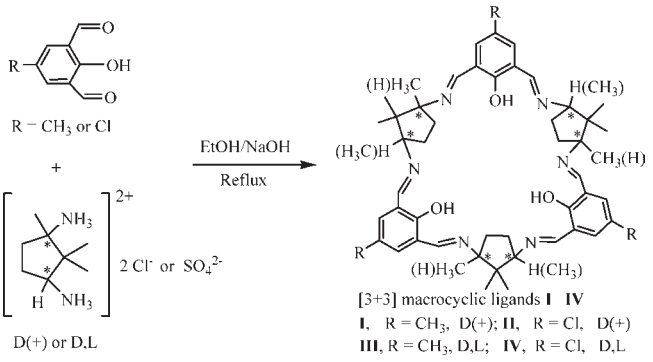

[a] The chiral carbon atoms are marked with asterisks.

2. Experimental Section

2.1. Materials and Measurements. Hydrochloride and sulfate salts of enantiopure and racemic 1,2,2-trimethylcyclopentane-1,3-diamine were prepared from D-(+)-camphoric acid and D,L-camphoric acid, respectively, via a literature method.[21] 2,6-Diformyl-4-substituted phenols (R = CH_3 or Cl) were prepared by an improved oxidation method using activated manganese(IV) dioxide from 4-R-2,6-bis(hydroxymethyl)phenols (R = CH_3 or Cl).[22−24] The other reagents of analytical grade were purchased from commercial sources and used without any further purification.

Elemental analyses were measured with a Perkin-Elmer 1400C analyzer. IR spectra (4000−400 cm^{-1}) were collected on a Nicolet FT-IR 170X spectrophotometer at 25 °C using KBr plates. Ultraviolet−visible (UV−vis) spectra were recorded on a Shimadzu UV-3100 double-beam spectrometer using a Pyrex cell with a path length of 10 mm at room temperature. The circular dichroism (CD) spectra were measured with a Jasco J-810 spectropolarimeter using the same solutions as those for the UV−vis determination. ^{1}H NMR spectroscopic measurements were performed on a Bruker AM-500 NMR spectrometer, using tetramethylsilane ($SiMe_4$) as an internal reference at room temperature. Electrospray ionization mass spectrometry (ESI-MS) spectra were recorded on a Finnigan MAT SSQ 710 mass spectrometer in a scan range of 100−1200 amu. Luminescence spectra were recorded on a Hitachi 850 fluorescent spectrophotometer at room temperature (25 °C).

2.2. Preparation of the Schiff-Base Ligands I−IV. [3 + 3] macrocyclic ligands **I** (R = CH_3, D-(+)-camphoric diamine), **II** (R = Cl, D-(+)-camphoric diamine), **III** (R = CH_3, D,L-camphoric diamine), and **IV** (R = Cl, D,L-camphoric diamine) were synthesized via the sodium(I) template Schiff-base condensation of corresponding dialdehydes and camphoric diamines, as illustrated in Scheme 1.

General Synthetic Method. An ethanol suspension of a hydrochloride (or sulfate) salt of D-(+)- (or D,L-) camphoric diamine

(16) (a) Gregoliński, J.; Starynowicz, P.; Hua, K. T.; Lunkley, J. L.; Muller, G.; Lisowski, J. *J. Am. Chem. Soc.* **2008**, *130*, 17761–17773. (b) Erxleben, A. *Coord. Chem. Rev.* **2003**, *246*, 203–248.

(17) (a) Huang, W.; Gou, S. H.; Hu, D. H.; Chantrapromma, S.; Fun, H. K.; Meng, Q. J. *Inorg. Chem.* **2001**, *40*, 1712–1715. (b) Gou, S. H.; Qian, M.; Yu, Z.; Duan, C. Y.; Sun, X. F.; Huang, W. *J. Chem. Soc., Dalton Trans.* **2001**, *21*, 3232–3237. (c) Huang, W.; Gou, S. H.; Hu, D. H.; Chantrapromma, S.; Fun, H. K.; Meng, Q. J. *Inorg. Chem.* **2002**, *41*, 864–868. (d) Huang, W.; Hu, D. H.; Gou, S. H.; Chantrapromma, S.; Fun, H. K.; Xu, Y.; Meng, Q. J. *Inorg. Chim. Acta* **2003**, *342*, 9–15. (e) Huang, W.; Gou, S. H.; Qian, H. F.; Hu, D. H.; Chantrapromma, S.; Fun, H. K.; Meng, Q. J. *Eur. J. Inorg. Chem.* **2003**, 947–954. (f) Huang, W.; Chu, Z. L.; Gou, S. H.; Ogawa, T. *Polyhedron* **2007**, *26*, 1483–1492.

(18) (a) Korupoju, S. R.; Zacharias, P. S. *Chem. Commun.* **1998**, 1267–1268. (b) Korupoju, S. R.; Mangayarkarasi, N.; Sardar, A.; Valente, E. J.; Zacharias, P. S. *J. Chem. Soc., Dalton Trans.* **2000**, 2845–2852. (c) Korupoju, S. R.; Mangayarkarasi, N.; Zacharias, P. S.; Mizuthani, J.; Nishihara, H. *Inorg. Chem.* **2002**, *41*, 4099–4101.

(19) (a) Chu, Z. L.; Huang, W.; Wang, L.; Gou, S. H. *Polyhedron* **2008**, *27*, 1079–1092. (b) Huang, W.; Chu, Z. L.; Jiang, J. C. *Polyhedron* **2008**, *27*, 2705–2709.

(20) (a) Qian, H. F.; Huang, W.; Gou, S. H. *J. Mol. Struct.* **2003**, *658*, 65–70. (b) Huang, W.; Zhou, Y. S.; Li, H. H.; Qian, H. F.; Gou, S. H. *Chin. J. Inorg. Chem.* **2004**, *20*, 205–209. (c) Huang, W.; Qian, H. F.; Gou, S. H.; Yao, C. *J. Mol. Struct.* **2005**, *743*, 185–192. (d) Qian, H. F.; Chu, Z. L.; Huang, W.; Liu, J. L. *J. Mol. Struct.* **2007**, *840*, 38–43. (e) Chu, Z. L.; You, W.; Fan, Y.; Qian, H. F.; Huang, W. *J. Coord. Chem.* **2009**, *62*, 2086–2094. (f) Wang, L.; You, W.; Huang, W.; Wang, C.; You, X. Z. *Inorg. Chem.* **2009**, *48*, 4295–4305. (g) Fan, Y.; You, W.; Huang, W.; Liu, J. L.; Wang, Y. N. *Polyhedron* **2010**, *29*, 1149–1155.

(21) (a) Yang, Z. H.; Wang, L. X.; Zhou, Z. H.; Zhou, Q. L.; Tang, C. C. *Tetrahedron: Asymmetry* **2001**, *12*, 1579–1582. (b) Chu, Z. L.; Fan, Y.; Huang, W.; Liu, J. L. *Acta Crystallogr.* **2007**, *E63*, o4927.

(22) Jiang, J. C.; Wang, G.; You, W.; Huang, W. *Acta Crystallogr.* **2008**, *E64*, o1426.

(23) Huang, W.; Gou, S. H.; Hu, D. H.; Meng, Q. J. *Synth. Commun.* **2000**, *30*, 1555–1561.

(24) Chu, Z. L.; Huang, W.; Gou, S. H. *Acta Crystallogr.* **2005**, *E61*, o1624–o1624.

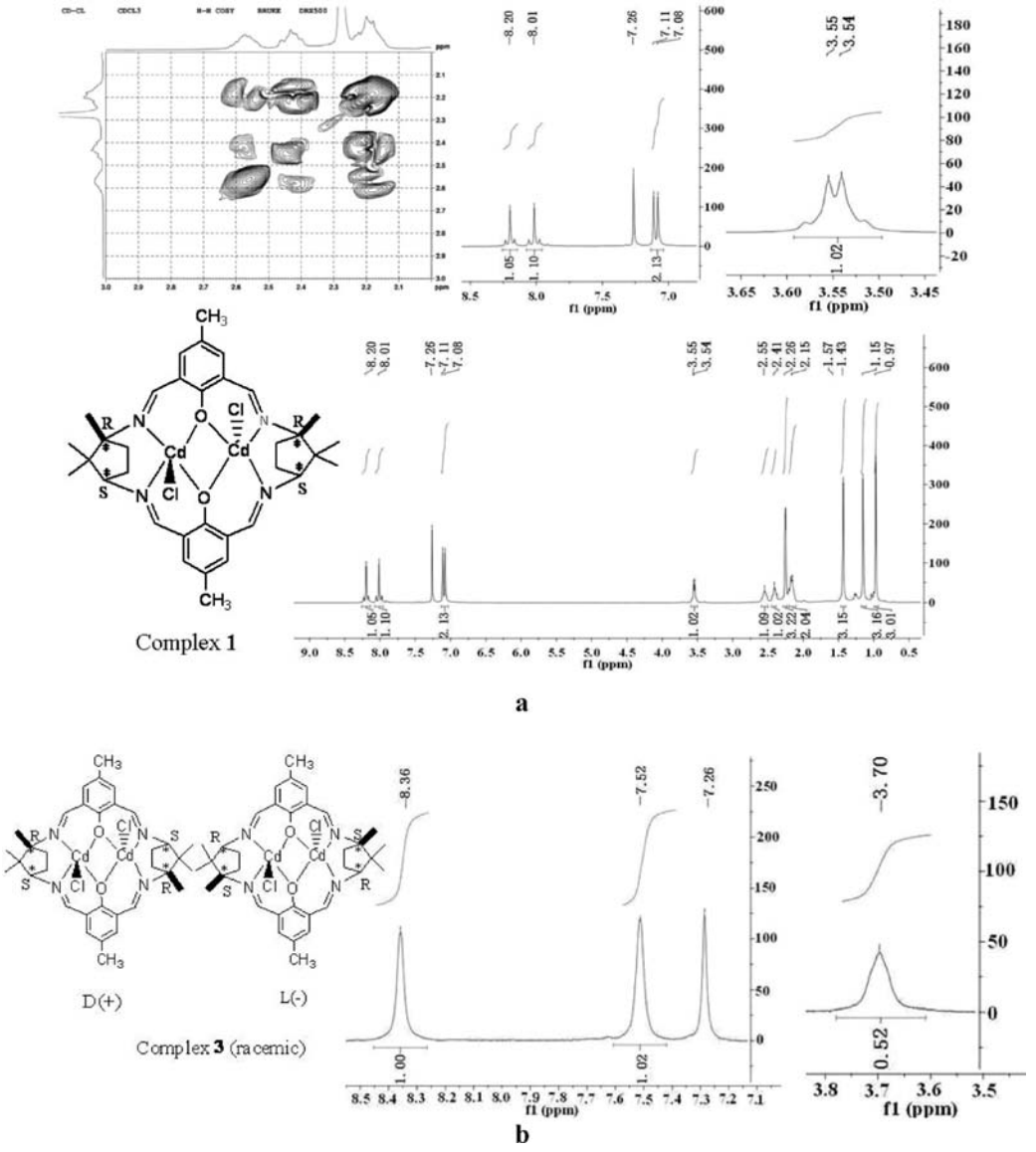

Figure 1. ^{1}H NMR spectra of [2 + 2] dinuclear cadmium(II) complexes **1** (a) and **3** (b) with enantiopure or racemic macrocyclic ligands.

(0.100 mmol, 0.0214 or 0.0240 g) was adjusted to pH = 7−8 with NaOH; then the mixture was filtered, and the filtrate was added slowly into an ethanol solution of sodium 4-R-2,6-diformylphenolate (R = CH_3 or Cl; 0.100 mmol, 0.0164 or 0.0184 g). After refluxing for 4−5 h, the mixture was filtered and the filtrate was concentrated on a rotary evaporator to obtain the [3 + 3] macrocyclic ligand as a yellow powder. Finally, the yellow powder was recrystallized by ethanol to obtain a crude product containing the [3 + 3] macrocyclic ligand. However, it is very difficult and time-consuming for us to obtain the pure [3 + 3] Schiff-base macrocyclic ligands of **I**−**IV** and get satisfactory ^{1}H NMR spectral data. The characterizations of four Schiff-base macrocyclic ligands are shown in the Supporting Information for reference.

2.3. Preparation of the Transition-Metal Complexes 1−12. Complexes 1−3. A solution of $CdCl_2$ (0.0551 g, 0.300 mmol) in methanol (10 cm^3) was added dropwise to a methanol solution (20 cm^3) of ligand **I** (0.0811 g, 0.100 mmol), ligand **II** (0.0872 g, 0.100 mmol), or ligand **III** (0.0811 g, 0.100 mmol). After 2 h of reflux, the corresponding mixture was cooled to room temperature and left in air for slow evaporation, giving light-yellow crystals of **1**−**3** suitable for X-ray diffraction determination after several days (Figure 1). Complex **1**: yield 0.0671 g (54% based on metal). Anal. Calcd for $Cd_2C_{34}H_{42}Cl_2N_4O_2$: C, 48.94; H, 5.07; N, 6.71. Found: C, 48.76; H, 5.32; N, 6.59. Main FT-IR absorptions (KBr pellets, cm^{-1}): 3440 (m), 2950 (m), 1670 (m), 1628 (s), 1550 (s), 1445 (m), 1404 (m), 1389 (m), 1329 (m), 1224 (m), 1040 (m), 996 (w). ^{1}H NMR (500 MHz, $CDCl_3$): δ 8.20 (2H, s, HC═N), 8.01 (2H, s, HC═N), 7.11 (2H, s, ArH), 7.08 (2H, s, ArH), 3.54 (2H, d, NCH), 2.55 (2H, m, CH_2CH_2), 2.41 (2H, m, CH_2CH_2), 2.26 (6H, s, $ArCH_3$), 2.15 (4H, m, CH_2CH_2), 1.43 (6H, s, CH_3), 1.15 (6H, s, CH_3), 0.97 (6H, s, CH_3). ESI-MS in methanol: $\{[2+2] - Cl^-\}^+$ m/z 799.1 (100%). UV−vis in methanol: λ_{max} = 372 and 251 nm. CD in methanol: λ_{max}= 397 (negative) and 269 (negative) nm. Fluorescence emission in methanol: λ_{max} = 439 nm. Complex **2**. Yield: 0.0758 g (58% based on metal). Anal. Calcd for $Cd_2C_{32}H_{36}Cl_4N_4O_2$: C, 43.91; H, 4.15; N, 6.40. Found: C, 46.88; H, 3.49; N, 5.56. Main FT-IR absorptions (KBr pellets, cm^{-1}): 3441 (m), 2971 (m), 1635 (s), 1581 (m), 1444 (s), 1385 (m), 1332 (m), 1217 (m), 1040 (m), 1035 (m), 987 (w). ^{1}H NMR (500 MHz, DMSO-d_6): δ 8.35 (2H, s, HC═N), 8.34 (2H, s, HC═N), 7.48 (2H, s, ArH), 7.34 (2H, s, ArH), 3.70 (2H, d, NCH), 1.94−2.43 (8H, m, CH_2CH_2), 1.44 (6H, s, CH_3), 1.13 (6H, s, CH_3), 0.86 (6H, s, CH_3). ESI-MS in methanol: $\{[1 + 2] - 2Cl^- + H\}^+ m/z$ 656.2 (100%). UV−vis in methanol: λ_{max} = 433, 363, and 202 nm. CD in methanol: λ_{max} = 442

(negative), 392 (negative), and 273 (negative) nm. Fluorescence emission in methanol: λ_{max} = 434 nm. Complex **3**. Yield: 0.0778 g (62% based on metal). Anal. Calcd for $Cd_2C_{34}H_{42}Cl_2N_4O_2$: C, 48.94; H, 5.07; N, 6.71. Found: C, 48.73; H, 5.19; N, 6.53. Main FT-IR absorptions (KBr pellets, cm^{-1}): 3448 (m), 2878 (m), 1628 (s), 1578 (s), 1445 (s), 1390 (m), 1330 (m), 1224 (m), 1109 (m), 1041 (m), 933 (w). ^{1}H NMR (500 MHz, $CDCl_3$): δ 8.34 (4H, s, HC=N), 7.29 (4H, s, ArH), 3.70 (2H, d, NCH), 2.34 (6H, s, $ArCH_3$), 1.97−2.26 (8H, m, CH_2CH_2), 1.44 (6H, s, CH_3), 1.13 (6H, s, CH_3), 0.86 (6H, s, CH_3). UV−vis in methanol: λ_{max} = 369 and 251 nm. Fluorescence emission in methanol: λ_{max} = 436 nm.

Complexes 4 and 5. A solution of $Cd(OAc)_2\cdot 2H_2O$ (0.0780 g, 0.300 mmol) or $CdBr_2\cdot 4H_2O$ (0.1032 g, 0.300 mmol) in methanol (10 cm^3) was added dropwise to a methanol solution (20 cm^3) of ligand **II** (0.0872 g, 0.100 mmol) or ligand **III** (0.0811 g, 0.100 mmol). After 2 h of reflux, the mixing solution was cooled to room temperature and left in air for several days, respectively, giving a light-yellow powder of **4** and a yellow powder of **5**. Single-crystal samples suitable for X-ray diffraction measurement were grown from a mixture of *N*,*N*-dimethylformamide (DMF)/methanol (**4**) and methanol (**5**) by slow evaporation in air at room temperature. Complex **4**. Yield: 0.0844 g (60% based on metal). Anal. Calcd for $C_{36}H_{42}Cd_2Cl_2N_4O_6\cdot C_3H_7NO\cdot 2H_2O$: C, 45.41; H, 5.18; N, 6.79. Found: C, 45.68; H, 5.55; N, 6.58. Main FT-IR absorptions (KBr pellets, cm^{-1}): 3448 (m), 2958 (m), 1630 (s), 1544 (m), 1439 (m), 1403 (m), 1331 (m), 1215 (m), 1160 (m), 1037 (m), 775 (w). ^{1}H NMR (500 MHz, DMSO-d_6): δ 8.48 (2H, s, HC=N), 8.37 (2H, s, HC=N), 7.90 (2H, s, ArH), 7.68 (2H, s, ArH), 3.70 (2H, d, NCH), 1.86−2.20 (8H, m, CH_2CH_2), 1.51 (s, 6H, OAc), 1.44 (6H, s, CH_3), 1.10 (6H, s, CH_3), 0.85 (6H, s, CH_3). ESI-MS in methanol/acetonitrile: $\{[1 + 1] + CH_3CN\}^+$ *m*/*z* 689.2 (100%). UV−vis in methanol: λ_{max} = 440, 329, and 202 nm. Fluorescence emission in methanol: λ_{max} = 476 nm. Complex **5**. Yield: 0.0819 g (58% based on metal). Anal. Calcd for $Cd_2C_{34}H_{44}Br_2N_4O_3$: C, 43.38; H, 4.71; N, 5.95. Found: C, 43.44; H, 4.99; N, 6.12. Main FT-IR absorptions (KBr pellets, cm^{-1}): 3449 (m), 2873 (m), 1626 (s), 1546 (s), 1459 (m), 1405 (m), 1331 (m), 1222 (m), 1160 (m), 1040 (m), 810 (w). ^{1}H NMR (500 MHz, DMSO-d_6): δ 8.33 (2H, s, HC=N), 8.29 (2H, s, HC=N), 7.48 (2H, s, ArH), 7.33 (2H, s, ArH), 3.69 (2H, d, NCH), 2.25 (6H, s, $ArCH_3$), 1.86−2.20 (8H, m, CH_2CH_2), 1.44 (6H, s, CH_3), 1.13 (6H, s, CH_3), 0.87 (6H, s, CH_3). ESI-MS in methanol: $\{[2 + 2] - Br^-\}^+$ *m*/*z* 861.0 (32%); $\{[1 + 2] - H_2O - HBr - Br^-\}^+$ *m*/*z* 633.2 (63%). UV−vis in methanol: λ_{max} = 386 and 258 nm. CD in methanol: λ_{max} = 397 (negative) and 255 (negative) nm. Fluorescence emission in methanol: λ_{max} = 499 nm.

Complex 6. A solution of $CdBr_2\cdot 4H_2O$ (0.1032 g, 0.300 mmol) in methanol (10 cm^3) was added dropwise to a methanol solution (20 cm^3) containing ligand **III** (0.0811 g, 0.100 mmol). The mixture was stirred at room temperature for 5 h and condensed to nearly 5 cm^3 with a rotatory evaporator. Dark-brown single-crystal samples of **6** suitable for X-ray diffraction measurement were grown from DMF by slow evaporation in air at room temperature. The yield is 0.0486 g (34% based on metal). Anal. Calcd for $Cd_2C_{25}H_{39}Br_3N_4O\cdot C_3H_7NO$: C, 35.43; H, 4.88; N, 7.38. Found: C, 35.31; H, 4.97; N, 7.31. Main FT-IR absorptions (KBr pellets, cm^{-1}): 3448 (b), 2872 (m), 1638 (s), 1545 (s), 1407 (m), 1327 (m), 1224 (m), 1145 (w), 1040 (s), 814 (w). ^{1}H NMR (500 MHz, DMSO-d_6): δ 8.34 (1H, s, HC=N), 8.30 (1H, s, HC=N), 7.49 (1H, s, ArH), 7.34 (1H, s, ArH), 3.69 (2H, d, NCH), 2.56 (4H, m, NH_2), 2.26 (3H, s, $ArCH_3$), 2.25 (2H, m, CH_2CH_2), 2.20 (2H, m, CH_2CH_2), 2.09 (2H, m, CH_2CH_2), 1.83 (2H, m, CH_2CH_2), 1.44 (6H, s, CH_3), 1.13 (6H, s, CH_3), 0.86 (6H, s, CH_3). ESI-MS in methanol: $\{[2 + 2] - 3HBr + Na\}^+$ *m*/*z* 661.2 (100%). UV−vis in methanol: λ_{max} = 385 and 257 nm. Fluorescence emission in methanol: λ_{max} = 492 nm.

Complexes 7−10. The syntheses of **7**−**10** were similar to that of **2** except that the metal salts were replaced by $ZnCl_2$ (0.0409 g, 0.300 mmol), $Zn(NO_3)_2\cdot 6H_2O$ (0.0893 g, 0.300 mmol), $MnCl_2$ (0.0378 g, 0.300 mmol), and $Mn(OAc)_2\cdot 4H_2O$ (0.0735 g, 0.300 mmol). In the cases of **8** and **10**, KSCN (0.0292 g, 0.300 mmol) was added into the mixing solutions after 2 h of reflux. The mixing solutions of **7**−**10** were cooled to room temperature, and the solvents were removed to obtain a light-yellow powder of **7** and **8** and a brown powder of **9** and **10**, respectively. Single crystals of **7**−**10** suitable for X-ray diffraction measurement were grown from a mixture of methanol and acetonitrile in a ratio of 2:1, 1:1, 1:2, or 1:1 (v/v) by slow evaporation in air at room temperature. Complex **7**. Yield: 0.0744 g (60% based on metal). Anal. Calcd for $Zn_2C_{32}H_{36}Cl_4N_4O_2$: C, 49.66; H, 4.78; N, 8.52. Found: C, 49.43; H, 5.34; N, 8.61. Main FT-IR absorptions (KBr pellets, cm^{-1}): 3423 (m), 2970 (m), 1670 (m), 1637 (s), 1557 (s), 1449 (m), 1412 (m), 1392 (m), 1331 (m), 1214 (m), 1041 (m), 773 (w). ^{1}H NMR (500 MHz, $CDCl_3$): δ 8.24 (2H, s, HC=N), 7.99 (2H, s, HC=N), 7.34 (2H, s, ArH), 7.28 (2H, s, ArH), 3.58 (2H, t, NCH), 2.45 (6H, m, CH_2CH_2), 2.13 (2H, m, CH_2CH_2), 2.01 (3H, s, CH_3CN), 1.45 (6H, s, CH_3), 1.15 (6H, s, CH_3), 0.99 (6H, s, CH_3). ESI-MS in methanol: $\{[2 + 2] + CH_3CN + H_2O - HCl - Cl^-\}^+$ *m*/*z* 769.3 (100%); $\{[2 + 2] + CH_3CN - Cl^-\}^+$ *m*/*z* 785.0 (35%). UV−vis in methanol: λ_{max} = 370, 248, and 202 nm. CD in methanol: λ_{max} = 393 (negative) and 266 (negative) nm. Complex **8**. Yield: 0.0772 g (57% based on metal). Anal. Calcd for $Zn_2C_{34}H_{36}Cl_2N_6O_2S_2\cdot 2CH_3CN$: C, 50.23; H, 4.66; N, 12.33. Found: C, 50.08; H, 4.76; N, 12.45. Main FT-IR absorptions (KBr pellets, cm^{-1}): 3259 (m), 3080 (m), 1693 (m), 1636 (s), 1568 (s), 1439 (m), 1414 (m), 1395 (m), 1361 (m), 1224 (m), 1031 (m), 742 (w). ^{1}H NMR (500 MHz, $CDCl_3$): δ 8.26 (2H, s, HC=N), 8.01 (2H, s, HC=N), 7.40 (2H, s, ArH), 7.34 (2H, s, ArH), 3.60 (2H, d, NCH), 2.54 (2H, m, CH_2CH_2), 2.31 (2H, m, CH_2CH_2), 2.17 (4H, m, CH_2CH_2), 1.60 (6H, s, CH_3), 1.47 (6H, s, CH_3), 0.98 (6H, s, CH_3). ESI-MS in methanol: $\{[2 + 2] - SCN^-\}^+$ *m*/*z* 769.1 (100%); $\{[2 + 2] + 2CH_3CN - SCN^-\}^+$ *m*/*z* 965.4 (66%). UV−vis in methanol: λ_{max} = 364, 223, and 202 nm. Complex **9**. Yield: 0.0661 g (58% based on metal). Anal. Calcd for $Mn_2C_{32}H_{36}Cl_4N_4O_2$: C, 50.55; H, 4.77; N, 7.37. Found: C, 49.76; H, 4.81; N, 7.62. Main FT-IR absorptions (KBr pellets, cm^{-1}): 3407 (m), 2973 (m), 1660 (m), 1638 (s), 1527 (s), 1441 (m), 1395 (m), 1325 (m), 1294 (m), 1215 (m), 1024 (m), 774 (w). ESI-MS in methanol: $\{[2 + 2] + H\}^+$ *m*/*z* 762.8 (100%). UV−vis in methanol: λ_{max} = 431, 340, and 202 nm. CD in methanol: λ_{max} = 433 (positive) and 342 (positive) nm. Complex **10**. Yield: 0.0732 g (55% based on metal). Anal. Calcd for $Mn_2C_{34}H_{36}Cl_2N_6O_2S_2\cdot 2CH_3CN$: C, 51.41; H, 4.77; N, 12.62. Found: C, 50.38; H, 4.65; N, 12.75. Main FT-IR absorptions (KBr pellets, cm^{-1}): 3408 (m), 2968 (m), 2048 (m), 1636 (s), 1541 (s), 1430 (m), 1414 (m), 1210 (m), 1035 (m), 747 (w). ESI-MS in methanol: $\{[2 + 2] + 2CH_3CN + H_2O - SCN^-\}^+$ *m*/*z* 767.2 (100%). UV−vis in methanol: λ_{max} = 382 and 202 nm. CD in methanol: λ_{max} = 433 (positive) and 261 (negative) nm.

Complexes 11 and 12. A solution of $Ni(NO_3)_2\cdot 6H_2O$ (0.0872 g, 0.300 mmol) or $CuCl_2\cdot 2H_2O$ (0.0511 g, 0.300 mmol) in methanol (10 cm^3) was added dropwise to a methanol solution (20 cm^3) containing ligand **IV** (0.0872 g, 0.100 mmol). The resulting mixture was stirred at room temperature for about 5 h and condensed to nearly 5 cm^3 with a rotatory evaporator. Green single-crystal samples of **11** and **12** suitable for X-ray diffraction measurement were grown from DMF by slow evaporation in air at room temperature. The bridging Cl^- ions in **11** were believed to come from the impurity (hydrochloride salt of camphoric diamine) in ligand **IV**. Complex **11**. Yield: 0.0558 g (42%) based on metal. Anal. Calcd for $C_{48}H_{60}Cl_4N_6Ni_3O_6\cdot 2NO_3\cdot 4H_2O$: C, 43.31; H, 5.15; N, 8.42. Found: C, 44.38; H, 4.75; N, 7.75. Main FT-IR absorptions (KBr pellets, cm^{-1}): 3418 (m), 3225 (m), 2968 (m), 1624 (s), 1561 (m), 1439 (m), 1384 (m), 1294 (m), 1225

(m), 1046 (m), 776 (w). ESI-MS in methanol: $\{M - 2NO_3^-\}^{2+}/2$ m/z 570.4 (100%). UV−vis in methanol: λ_{max} = 360 and 202 nm. Complex **12**. Yield: 0.0234 g. Main FT-IR absorptions (KBr pellets, cm^{-1}): 3423 (m), 3218 (m), 2971 (m), 1636 (s), 1558 (s), 1458 (m), 1420 (m), 1380 (m), 1323 (m), 1226 (m), 1078 (m), 1044 (m), 746 (w). ESI-MS in methanol: $\{M - 2NO_3^- + H\}^+$ m/z 1137.1 (17%); $\{M - 2Cl^-$ − one camphoric diamine unit$\}^{2+}/2$ m/z 616.9 (100%). UV−vis in methanol: λ_{max} = 358 and 202 nm.

2.4. X-ray Data Collection and Structural Determination. Single-crystal samples of **1**−**12** were glue-covered and mounted on glass fibers and then used for data collection. Crystallographic data of **6** and **12** were collected on a Rigaku Mercury CCD area detector, while the other 10 samples were collected on a Bruker SMART 1K CCD diffractometer, using graphite-monochromated Mo Kα radiation (λ = 0.710 73 Å). In the cases of **6** and **12**, the original data files generated by *CRYSTALCLEAR* were transformed to *SHELXTL97* format by the *TEXSAN* program.[25,26] The crystal systems were determined by Laue symmetry, and the space groups were assigned on the basis of systematic absences using XPREP. Absorption corrections were performed to all data, and the structures were solved by direct methods and refined by a full-matrix least-squares method on F_o^2 by using the *SHELXTL-PC* software package.[27] All non-hydrogen atoms were anisotropically refined, and all hydrogen atoms were inserted in the calculated positions, assigned fixed isotropic thermal parameters, and allowed to ride on their respective parent atoms. In the case of **12**, the main structure (cation) can be easily solved, but the severely disordered anions and solvent molecules are very difficult to fully locate because of the very low-quality diffraction data even though many attempts were carried out and the data were collected at 100(2) K and in the maximum power of the Rigaku system. A summary of the crystal data, experimental details, and refinement results for **1**−**11** is listed in Table 1, whereas selected bond distances and angles related to the metal centers are given in Table 2

3. Results and Discussion

3.1. Syntheses. The macrocyclic ligands **I**−**IV** were synthesized via Schiff-base condensation between 2,6-diformyl-4-substituted phenol (R = CH_3 or Cl) and D-(+)- or D,L-1,2,2-trimethylcyclopentane-1,3-diamine in the presence of a sodium ion as the template agent. Similar to the syntheses of enantiomeric [(1*R*,2*R*) or (1*S*,2*S*)] and racemic *trans*-cyclohexane-1,2-diamine Schiff-base macrocycles,[18,19] [3 + 3] Schiff-base macrocycles have been proven to be the main products (Scheme 1). Positive ESI-MS diagrams of ligands **I**−**IV** in their ethanol solutions indicate peaks in agreement with the presence of [3 + 3] Schiff-base macrocyclic species. For example, the enantiopure [3 + 3] Schiff-base macrocyclic ligand **II** gives two predominant ESI-MS peaks centered at m/z 873.3 and 437.3, respectively (Figure SI1 in the Supporting Information). The former is assigned to the molecular peak of **II** with 100% abundance, and the latter is attributed to the doubly charged peak of **II** with 75% abundance. In addition, two peaks, at m/z 581.3 (18%) and 291.3 (25%), are observed, confirming the production of molecular and doubly charged peaks of [2 + 2] Schiff-base macrocycles.

However, the [3 + 3] Schiff-base macrocyclic ligands are not stable when treated with some transition-metal ions, such as cadmium(II), zinc(II), manganese(II), nickel(II), and copper(II) ions, where cleavage of the C=N double bond in their molecular structures and subsequent ring degradation take place. They are mainly due to the reversible formation and decomposition of Schiff-base units in the macrocyclic ligands as well as the size effects and coordination geometric requirements of the metal centers. Nevertheless, some other factors can also influence the resulting products such as steric hindrance of the ligands, the presence of different counterions, and alteration of the experimental conditions. Resultantly, planar dinuclear complexes are proven to be the main products (complexes **1**−**10** in Scheme 2). Generally, a reflux condition is used to prepare the [2 + 2] macrocyclic metal complexes, which are suggested to be the most thermally stable products. In contrast, when the reaction is carried out at room temperature, the products are complicated and both macrocyclic and acyclic complexes could be yielded. For instance, [2 + 2] macrocyclic complex **5** is prepared in a reflux condition, while the [1 + 2] acyclic complex **6** can be isolated with a relatively lower yield in a room temperature reaction.

In our experiments, Schiff-base metal−organic complexes can also be prepared via a more conventional in situ method, where appropriate sodium 2,6-diformyl-4-substituted phenate, camphoric diamine, and metal salt are used in an equal molar ratio. However, it should be mentioned that the use of different salts of camphoric diamine (hydrochloride and sulfate salts) in the course of metal-ion complexation produces different products. It is found that the chloride anion preferentially coordinates with the central metal ions because of its stronger coordination ability when hydrochloride salts of camphoric diamine are used, which can be further verified by the formation of multinuclear complexes **11** and **12** bearing μ_2- and μ_3-Cl^- bridges (Scheme 2b). However, this can be avoided by the replacement of sulfate salts of camphoric diamine as the starting material. As a result, different kinds of apical ligands (Br^-, OAc^-, SCN^-, and H_2O) can coordinate with the central metal ions in the cases of dinuclear species, which may originate from the weaker coordination ability of the SO_4^{2-} anion.

3.2. Spectral Characterizations for the Macrocyclic Ligands and Their Transition-Metal Complexes. The FT-IR spectra of macrocyclic ligands **I**−**IV** display sharp peaks at 1635, 1632, 1633, and 1639 cm^{-1}, indicative of the presence of a Schiff-base C=N double bond. Additionally, medium peaks at 2870−2972 and 1375−1376 cm^{-1} have been observed, characteristic of the absorptions for alkyl groups of camphoric diamine units in the macrocyclic ligands.

In UV−vis spectra, Cl-substituted species (macrocyclic ligands **II** and **IV** and complexes **2**, **4**, and **7**−**12**) reveal a very strong absorption peak around 202 nm, so their methanol solutions with higher concentrations are used to distinguish the low-energy band absorptions from the corresponding CH_3-substituted ones. As shown in Figure SI2 in the Supporting Information, macrocyclic ligands **I**−**IV** have two intense absorptions in their electronic

(25) Molecular Structure Corporation and Rigaku Corporation. *CRYSTALCLEAR*, version 1.3; MSC and Rigaku: The Woodlands, TX , and Tokyo, **2001**.

(26) Molecular Structure Corporation and Rigaku Corporation. *TEXSAN*, version 1.11; MSC and Rigaku: The Woodlands, TX and Tokyo, **2000**.

(27) Sheldrick, G. M. *SHELXTL: Software Reference Manual*, version 6.10; Bruker AXS, Inc.: Madison, WI, **2000**.

Table 1. Crystallographic Data and Structure Refinements for Complexes **1**−**11**

	1	**2**	**3**	**4**	**5**	**6**
formula	$C_{34}H_{42}Cd_2Cl_2N_4O_2$	$C_{64}H_{72}Cd_4Cl_8N_8O_4$	$C_{57}H_{76}Cd_3Cl_3N_8O_5$	$C_{39}H_{53}Cd_2Cl_2N_5O_9$	$C_{34}H_{44}Br_2Cd_2N_4O_3$	$C_{28}H_{46}Br_3Cd_2N_5O_2$
fw	834.44	1750.50	1396.84	1031.58	941.35	949.22
T [K]	291(2)	291(2)	291(2)	291(2)	291(2)	291(2)
cryst size [mm]	0.10 × 0.12 × 0.16	0.10 × 0.10 × 0.16	0.10 × 0.15 × 0.20	0.10 × 0.10 × 0.12	0.10 × 0.10 × 0.10	0.10 × 0.10 × 0.12
cryst syst	monoclinic	monoclinic	triclinic	monoclinic	monoclinic	monoclinic
space group	$P2_1$	$P2_1$	$P\bar{1}$	$P2_1$	$P2_1$	$C2/c$
a [Å]	15.779(3)	15.771(2)	13.018(1)	10.981(1)	9.385(3)	38.131(8)
b [Å]	13.251(3)	13.249(2)	13.711(1)	14.893(1)	16.564(5)	8.874(2)
c [Å]	18.210(4)	18.210(3)	18.422(2)	14.049(1)	11.729(4)	24.899(5)
α [deg]	90	90	68.532(2)	90	90	90.00
β [deg]	111.450(2)	111.418(2)	77.304(2)	93.050(1)	105.117(5)	119.18(3)
γ [deg]	90	90	87.564(2)	90	90	90.00
V [Å^3]	3543.8(13)	3542.3(9)	2982.6(5)	2294.1(3)	1760.2(10)	7356(3)
ρ_{calcd} [g cm^{-3}]/Z	1.564/4	1.641/2	1.555/2	1.493/2	1.776/2	1.714/8
F(000)	1680	1744	1418	1048	932	3728
μ [mm^{-1}]	1.386	1.536	1.247	1.097	3.517	4.445
max/min h, k, l	10/−19, 16/−15, 22/−22	18/−15, 10/−15, 19/−21	15/−15, 13/−16, 21/−19	12/−13, 16/−17, 11/−16	9/−11, 19/−19, 13/−13	45/−45, 10/−10, 24/−29
collected reflns	19 275	18 084	14 843	11 687	2675	31 048
unique reflns	13 354	11 093	10 293	7173	1380	6434
reflns with $I > 2\sigma(I)$	11398	6324	7773	3897	2454	5355
no. of param	808	802	674	522	407	369
Flack parameter	−0.04(2)	−0.10(6)		0.04(6)	0.02(3)	
R1/wR2[a] [$I > 2\sigma(I)$]	0.0315/0.0641	0.0673/0.1697	0.0516/0.1406	0.0542/0.0938	0.0699/0.1442	0.0697/0.1501
R1/wR2[a] (all data)	0.0397/0.0666	0.1142/0.2545	0.0664/0.1471	0.1075/0.1044	0.1592/0.1638	0.0875/0.1579
GOF on F^2	0.96	0.93	1.00	0.95	0.98	1.18
max/min $\Delta\rho$ [e Å^{-3}]	0.82/−0.50	1.83/−0.88	1.66/−0.77	0.71/−0.52	1.78/−0.65	0.85/−0.94

	7	**8**	**9**	**10**	**11**
formula	$C_{34}H_{39}Cl_4Zn_2N_5O_2$	$C_{38}H_{42}Cl_2S_2Zn_2N_8O_2$	$C_{32}H_{36}Cl_4Mn_2N_4O_2$	$C_{38}H_{42}Cl_2Mn_2N_8O_2S_2$	$C_{48}H_{68}Cl_4N_8Ni_3O_{16}$
fw	822.28	908.62	760.33	887.72	1330.98
T [K]	291(2)	291(2)	291(2)	291(2)	291(2)
cryst size [mm]	0.10 × 0.12 × 0.14	0.12 × 0.12 × 0.14	0.10 × 0.12 × 0.14	0.10 × 0.10 × 0.12	0.15 × 0.20 × 0.20
cryst syst	orthorhombic	monoclinic	monoclinic	monoclinic	triclinic
space group	$P2_12_12_1$	$P2_1$	$P2_1$	$P2_1$	$P\bar{1}$
a [Å]	11.242(1)	10.352(9)	15.280(1)	10.435(2)	10.096(3)
b [Å]	15.744(2)	13.226(10)	13.320(1)	13.368(2)	14.177(4)
c [Å]	20.618(2)	15.015(10)	18.182(1)	14.919(2)	20.940(6)
α [deg]	90.00	90	90	90	95.563(5)
β [deg]	90.00	95.63(2)	110.48(1)	95.82(2)	99.788(5)
γ [deg]	90.00	90	90	90	94.268(5)
V [Å^3]	3649.5(6)	2046(3)	3466.7(5)	2070.5(5)	2927.0(15)
ρ_{calcd} [g cm^{-3}]/Z	1.497/4	1.475/2	1.457/4	1.424/2	1.510/2
F(000)	1688	936	1560	916	1384
μ [mm^{-1}]	1.645	1.449	1.071	0.883	1.209
max/min h, k, l	13/−13, 17/−18, 24/−18	12/−11, 15/−12, 17/−16	15/−18, 15/−15, 21/−13	10/−12, 15/−13, 17/−17	12/−11, 12/−16, 24/−23
collected reflns	18 653	9857	17 579	10 433	14 632
unique reflns	6426	6079	10 994	5731	10 114
reflns with $I > 2\sigma(I)$	4034	3792	7806	3270	6150
no. of param	425	493	799	495	721
Flack parameter	0.02(1)	−0.13(3)	−0.01(2)	−0.09(3)	
R1/wR2[a] [$I > 2\sigma(I)$]	0.0405/0.0649	0.0570/0.1374	0.0477/0.1051	0.0449/0.0835	0.0665/0.1367
R1/wR2[a] (all data)	0.0739/0.0729	0.0957/0.1804	0.0721/0.1307	0.0868/0.0989	0.1174/0.1541
GOF on F^2	0.79	1.03	0.99	0.87	0.95
max/min $\Delta\rho$ [e Å^{-3}]	0.42/−0.39	0.42/−0.46	0.32/−0.38	0.29/−0.28	1.02/−0.44

[a] $R1 = \sum||F_o| - |F_c||/\sum|F_o|$; $wR2 = [\sum[w(F_o^2 - F_c^2)^2]/\sum w(F_o^2)^2]^{1/2}$.

spectra analogous to our previously reported [3 + 3] *trans*-cyclohexane-1,2-diamine-based macrocycles.[19] Namely, **I** and **III** have the same peaks at 251 and 373 nm, while **II** and **IV** have peaks at 341 and 442 nm. The strong absorption bands at 251 and 341 nm are assigned to the $\pi-\pi^*$ transition of benzene rings, whereas the intense absorptions at 373 and 442 nm are attributed to the $\pi-\pi^*$ transition of an azomethine chromophore. In contrast, the CH_3- and Cl-substituted metal complexes **1**−**12** have absorptions analogous to those of the macrocyclic ligands, respectively (Table 3). In summary, the electronic spectra of these Schiff-base ligands and their transition-metal complexes demonstrate slight differences before and after the metal-ion complexation but significant changes for the CH_3- and Cl-substituent groups in the macrocyclic skeletons, which could be attributed to their dissimilar electron-donating and -withdrawing abilities.

In CD spectra of the related chiral dinuclear cadmium(II), zinc(II), and manganese(II) complexes **1**, **2**, **5**, **7**, **9**, and **10** in CH_3OH (the insets in Figure SI2 in the

Table 2. Selected Bond Lengths [Å] and Angles [deg] for Complexes **1**−**11**[a]

1		**2**		**3**		**4**		**5**		**6**	
Cd1−Cl1	2.406(2)	Cd1−Cl3	2.402(8)	Cd1−Cl	2.409(2)	Cd1−O1	2.274(11)	Cd1−Br1	2.531(3)	Cd1−Br1	2.809(2)
Cd1−O1	2.232(3)	Cd1−O1	2.213(16)	Cd1−O1	2.205(4)	Cd1−O2	2.230(9)	Cd1−O1	2.213(17)	Cd1−Br3	2.537(2)
Cd1−O2	2.240(3)	Cd1−O2	2.306(14)	Cd1−O1_a	2.239(4)	Cd1−O3	2.285(17)	Cd1−O2	2.224(13)	Cd1−O1	2.230(6)
Cd1−N1	2.310(4)	Cd1−N1	2.279(18)	Cd1−N1	2.249(6)	Cd1−O4	2.314(13)	Cd1−N1	2.254(18)	Cd1−N3	2.278(8)
Cd1−N2	2.244(4)	Cd1−N2	2.240(20)	Cd1−N2	2.302(5)	Cd1−N3	2.310(11)	Cd1−N2	2.355(17)	Cd1−N4	2.277(9)
Cd2−Cl2	2.418(2)	Cd2−Cl4	2.411(8)	Cd2−Cl2	2.411(2)	Cd1−N4	2.323(12)	Cd2−Br2	2.502(4)	Cd2−Br1	2.652(2)
Cd2−O1	2.208(3)	Cd2−O1	2.202(16)	Cd2−O2	2.256(4)	Cd2−O1	2.259(11)	Cd2−O1	2.272(14)	Cd2−Br2	2.554(2)
Cd2−O2	2.269(3)	Cd2−O2	2.243(15)	Cd2−O2_b	2.225(3)	Cd2−O2	2.253(10)	Cd2−O2	2.273(14)	Cd2−O1	2.323(5)
Cd2−N3	2.284(4)	Cd2−N3	2.267(18)	Cd2−N3	2.238(5)	Cd2−O5	2.310(13)	Cd2−O3	2.245(14)	Cd2−N1	2.262(7)
Cd2−N4	2.317(4)	Cd2−N4	2.270(20)	Cd2−N4	2.286(5)	Cd2−O6	2.207(17)	Cd2−N3	2.271(18)	Cd2−N2	2.343(8)
Cd3−O4	2.256(3)	Cd3−O3	2.207(12)	Cd3−Cl3	2.402(2)	Cd2−N1	2.297(12)	Cd2−N4	2.300(20)		
Cd3−Cl3	2.414(2)	Cd3−O4	2.236(15)	Cd3−O3	2.248(4)	Cd2−N2	2.313(12)				
Cd3−O3	2.229(4)	Cd3−Cl7	2.415(7)	Cd3−O3_c	2.234(3)						
Cd3−N5	2.334(5)	Cd3−N5	2.310(20)	Cd3−N5	2.265(5)						
Cd3−N6	2.239(4)	Cd3−N6	2.310(20)	Cd3−N6	2.280(5)						
Cd4−N7	2.259(3)	Cd4−O3	2.217(15)								
Cd4−Cl4	2.415(2)	Cd4−Cl8	2.386(7)								
Cd4−O3	2.223(4)	Cd4−N7	2.260(20)								
Cd4−N8	2.300(3)	Cd4−N8	2.372(18)								
Cd4−O4	2.300(4)	Cd4−O4	2.254(12)								
Cl1−Cd1−O1	108.6(1)	Cl3−Cd1−N1	118.4(5)	Cl1−Cd1−O1	114.7(1)	N3−Cd1−N4	86.2(4)	Br1−Cd1−O1	105.0(4)	Br1−Cd1−Br3	99.3(1)
Cl1−Cd1−O2	112.9(1)	Cl3−Cd1−N2	105.2(5)	Cl1−Cd1−O1_a	114.1(1)	N3−Cd1−C35	119.0(5)	Br1−Cd1−O2	120.1(3)	Br1−Cd1−O1	81.9(2)
Cl1−Cd1−N1	112.8(1)	Cl3−Cd1−O1	119.5(5)	Cl1−Cd1−N1	113.9(2)	N4−Cd1−C35	116.8(5)	Br1−Cd1−N1	120.4(4)	Br1−Cd1−N3	151.5(2)
Cl1−Cd1−N2	120.6(1)	Cl3−Cd1−O2	114.6(4)	Cl1−Cd1−N2	111.7(2)	O1−Cd1−C35	109.6(5)	Br1−Cd1−N2	109.4(4)	Br1−Cd1−N4	87.3(3)
O1−Cd1−O2	73.1(1)	N1−Cd1−N2	88.7(7)	O1−Cd1−O1_a	73.0(1)	O1−Cd1−N3	130.9(4)	O1−Cd1−O2	74.6(5)	Br3−Cd1−O1	117.8(1)
O1−Cd1−N1	80.7(2)	O1−Cd1−N1	84.0(6)	O1−Cd1−N1	130.7(2)	O1−Cd1−N4	77.4(4)	O1−Cd1−N1	134.6(6)	Br3−Cd1−N3	108.6(2)
O1−Cd1−N2	130.0(2)	O1−Cd1−N2	132.4(6)	O1−Cd1−N2	81.6(2)	O1−Cd1−O2	73.3(4)	O1−Cd1−N2	78.7(6)	Br3−Cd1−N4	121.3(3)
O2−Cd1−N1	132.5(1)	O1−Cd1−O2	72.2(6)	O1_a−Cd1−N1	80.5 (2)	O1−Cd1−O3	89.8(5)	O2−Cd1−N1	80.7(5)	O1−Cd1−N3	79.9(2)
O2−Cd1−N2	80.0(1)	O2−Cd1−N1	127.0(6)	O1_a−Cd1−N2	133.6(2)	O1−Cd1−O4	130.8(4)	O2−Cd1−N2	128.1(5)	O1−Cd1−N4	120.9(3)
N1−Cd1−N2	80.0(1)	O2−Cd1−N2	75.4(6)	N1−Cd1−N2	88.2(2	O2−Cd1−C35	112.7(5)	N1−Cd1−N2	87.9(7)	N3−Cd1−N4	83.5(3)
Cl2−Cd2−O1	111.2(1)	Cl4−Cd2−N3	119.7(5)	Cl2−Cd2−O2	113.5(1)	O2−Cd1−N3	82.2(4)	Br2−Cd2−O1	106.3(4)	Br1−Cd2−Br2	113.3(1)
Cl2−Cd2−O2	109.2(1)	Cl4−Cd2−N4	104.5(5)	Cl2−Cd2−O2_b	114.6(1)	O2−Cd1−N4	128.4(4)	Br2−Cd2−O2	116.4(3)	Br1−Cd2−O1	83.8(2)
Cl2−Cd2−N3	113.5(1)	Cl4−Cd2−O1	111.6(4)	Cl2−Cd2−N3	116.8(2)	O2−Cd1−O3	94.1(5)	Br2−Cd2−O3	166.3(4)	Br1−Cd2−N1	117.2(2)
Cl2−Cd2−N4	121.5(1)	Cl4−Cd2−O2	119.3(4)	Cl2−Cd2−N4	109.7(2)	O2−Cd1−O4	127.6(4)	Br2−Cd2−N3	121.8(5)	Br1−Cd2−N2	103.2(2)
O1−Cd2−O2	73.0(1)	N3−Cd2−N4	86.5(7)	O2−Cd2−O2_b	74.1(1)	O3−Cd1−C35	24.3(6)	Br2−Cd2−N4	115.2(4)	Br2−Cd2−O1	98.6(1)
O1−Cd2−N3	132.8(1)	O1−Cd2−N3	128.7(6)	O2−Cd2−N3	79.7(2)	O3−Cd1−N3	134.6(6)	O1−Cd2−O2	73.1(5)	Br2−Cd2−N1	128.6(2)
O1−Cd2−N4	82.1(1)	O1−Cd2−N4	81.3(6)	O2−Cd2−N4	136.1(2)	O3−Cd1−N4	127.4(5)	O1−Cd2−O3	60.0(5)	Br2−Cd2−N2	92.9(2)
O2−Cd2−N3	78.7(2)	O1−Cd2−O2	73.6(6)	O2_b−Cd2−N3	128.1(2)	O3−Cd1−O4	49.9(5)	O1−Cd2−N3	131.0(6)	O1−Cd2−N1	77.9(2)
O2−Cd2−N4	128.8(2)	O2−Cd2−N3	81.2(6)	O2_b−Cd2−N4	81.2(2)	O4−Cd1−C35	25.6(6)	O1−Cd2−N4	79.9(6)	O1−Cd2−N2	163.0(2)
N3−Cd2−N4	87.4(1)	O2−Cd2−N4	134.9(6)	N3−Cd2−N4	88.2(2)	O4−Cd1−N3	97.9(4)	O2−Cd2−O3	61.3(5)	N1−Cd2−N2	85.2(2)
O3−Cd3−N6	129.1(1)	Cl7−Cd3−N5	123.2(6)	Cl3−Cd3−O3	113.2(1)	O4−Cd1−N4	103.7(4)	O2−Cd2−N3	77.7(6)		
Cl3−Cd3−O3	111.2(1)	Cl7−Cd3−N6	112.8(5)	Cl3−Cd3−O3_c	114.5(1)	N1−Cd2−C33	118.0(5)	O2−Cd2−N4	126.5(5)		
Cl3−Cd3−O4	120.4(1)	Cl7−Cd3−O3	110.5(4)	Cl3−Cd3−N5	113.5(2)	N1−Cd2−N2	87.4(4)	O3−Cd2−N3	71.7(6)		
Cl3−Cd3−N5	104.6(1)	Cl7−Cd3−O4	107.9(5)	Cl3−Cd3−N6	113.7(2)	N2−Cd2−C33	117.4(5)	O3−Cd2−N4	65.2(5)		
Cl3−Cd3−N6	119.6(1)	N5−Cd3−N6	87.0(7)	O3−Cd3−O3_c	73.9(1)	O1−Cd2−C33	109.3(5)	N3−Cd2−N4	87.3(7)		
O3−Cd3−O4	73.7(1)	O3−Cd3−N5	82.0(6)	O3−Cd3−N5	79.7(2)	O1−Cd2−N1	77.8(4)				
O3−Cd3−N5	80.8(1)	O3−Cd3−N6	134.0(7)	O3−Cd3−N6	132.6(2)	O1−Cd2−N2	132.6(4)				
N5−Cd3−N6	87.1(2)	O3−Cd3−O4	72.8(5)	O3_c−Cd3−N5	131.2(2)	O1−Cd2−O2	73.2(4)				
O4−Cd3−N5	133.7(1)	O4−Cd3−N5	128.3(7)	O3_c−Cd3−N6	80.9(2)	O1−Cd2−O5	109.1(5)				
O4−Cd3−N6	80.3(1)	O4−Cd3−N6	80.0(6)	N5−Cd3−N6	88.1(2)	O1−Cd2−O6	113.6(7)				
O3−Cd4−N8	83.4(1)	Cl8−Cd4−N7	122.0(6)			O2−Cd2−C33	112.9(5)				
Cl4−Cd4−O3	120.0(1)	Cl8−Cd4−N8	111.1(5)			O2−Cd2−N1	127.3(4)				
Cl4−Cd4−O4	113.7(1)	Cl8−Cd4−O3	110.0(5)			O2−Cd2−N2	81.3(4)				
Cl4−Cd4−N7	103.5(1)	Cl8−Cd4−O4	114.3(5)			O2−Cd2−O5	135.9(5)				
Cl4−Cd4−N8	119.3(1)	N7−Cd4−N8	88.3(7)			O2−Cd2−O6	89.2(6)				
O3−Cd4−O4	73.0(1)	O3−Cd4−N7	127.2(7)			O5−Cd2−C33	23.2(6)				
O4−Cd4−N7	77.5(1)	O3−Cd4−N8	81.0(6)			O5−Cd2−N1	95.0(5)				
O4−Cd4−N8	127.0(1)	O3−Cd4−O4	72.7(5)			O5−Cd2−N2	116.9(6)				
N7−Cd4−N8	87.6(1)	O4−Cd4−N7	78.6(6)			O5−Cd2−O6	48.5(7)				
O3−Cd4−N7	134.3(1)	O4−Cd4−N8	132.8(6)			O6−Cd2−C33	25.9(7)				
						O6−Cd2−N1	143.2(6)				
						O6−Cd2−N2	105.1(7)				

7		**8**		**9**		**10**		**11**	
Zn1−Cl3	2.258(2)	Zn1−O1	2.063(7)	Mn1−Cl1	2.331(3)	Mn1−O1	2.107(4)	Ni1−Cl4	2.558(2)
Zn1−O1	2.067(3)	Zn1−O2	2.097(6)	Mn1−O1	2.085(5)	Mn1−O2	2.117(4)	Ni1−O1	2.000(4)
Zn1−O2	2.085(3)	Zn1−N1	2.087(9)	Mn1−O2	2.161(4)	Mn1−N1	2.201(5)	Ni1−O3	2.138(4)
Zn1−N1	2.108(5)	Zn1−N3	2.055(8)	Mn1−N1	2.230(5)	Mn1−N4	2.166(5)	Ni1−O4	2.083(3)
Zn1−N2	2.064(4)	Zn1−N5	1.999(14)	Mn1−N4	2.152(5)	Mn1−N5	2.077(7)	Ni1−N1	2.047(5)
Zn2−Cl4	2.244(2)	Zn2−O1	2.051(6)	Mn2−Cl2	2.363(2)	Mn2−O1	2.118(4)	Ni1−N2	2.075(4)
Zn2−O1	2.057(3)	Zn2−O2	2.087(7)	Mn2−O1	2.095(5)	Mn2−O2	2.117(4)	Ni2−Cl4	2.560(2)
Zn2−O2	2.107(3)	Zn2−N2	2.087(9)	Mn2−O2	2.156(4)	Mn2−N2	2.195(5)	Ni2−O4	2.002(4)

Table 2. Continued

7		8		9		10		11	
Zn2−N3	2.079(5)	Zn2−N4	2.093(11)	Mn2−N2	2.246(5)	Mn2−N3	2.154(6)	Ni2−O5	2.153(4)
Zn2−N4	2.147(4)	Zn2−N6	1.971(12)	Mn2−N3	2.151(5)	Mn2−N6	2.055(8)	Ni2−O6	2.084(4)
				Mn3−O3	2.105(4)			Ni2−N3	2.037(4)
				Mn3−O4	2.147(5)			Ni2−N4	2.089(5)
				Mn3−Cl5	2.343(2)			Ni3−Cl4	2.525(2)
				Mn3−N8	2.177(5)			Ni3−O1	2.060(4)
				Mn3−N5	2.225(7)			Ni3−O2	2.134(4)
				Mn4−O3	2.109(5)			Ni3−O6	1.987(4)
				Mn4−Cl6	2.343(2)			Ni3−N5	2.026(5)
				Mn4−N6	2.242(5)			Ni3−N6	2.075(6)
				Mn4−N7	2.172(7)				
				Mn4−O4	2.119(4)				
Cl3−Zn1−O1	105.4(1)	O1−Zn1−O2	75.7(3)	Cl1−Mn1−O1	113.5(2)	O1−Mn1−O2	76.4(2)	Cl4−Ni1−O1	81.0(1)
Cl3−Zn1−O2	103.0(1)	O1−Zn1−N1	89.7(3)	Cl1−Mn1−O2	107.4(1)	O1−Mn1−N1	85.8(2)	Cl4−Ni1−O3	160.2(1)
Cl3−Zn1−N1	111.2(1)	O1−Zn1−N3	144.8(4)	Cl1−Mn1−N1	116.6(2)	O1−Mn1−N4	141.1(2)	Cl4−Ni1−O4	78.3(1)
Cl3−Zn1−N2	106.1(1)	O1−Zn1−N5	106.6(4)	Cl1−Mn1−N4	101.6(2)	O1−Mn1−N5	111.3(2)	Cl4−Ni1−N1	100.9(1)
O1−Zn1−O2	74.3(1)	O2−Zn1−N1	150.2(4)	O1−Mn1−O2	75.2(2)	O2−Mn1−N1	143.1(2)	Cl4−Ni1−N2	99.6(1)
O1−Zn1−N1	88.6(14	O2−Zn1−N3	86.2(3)	O1−Mn1−N1	86.5(2)	O2−Mn1−N4	83.3(2)	O1−Ni1−O3	87.4(2)
O1−Zn1−N2	145.7(2)	O2−Zn1−N5	100.3(4)	O1−Mn1−N4	142.5(2)	O2−Mn1−N5	104.5(2)	O1−Ni1−O4	90.7(2)
O2−Zn1−N1	144.8(1)	N1−Zn1−N3	91.7(3)	O2−Mn1−N1	136.0(2)	N1−Mn1−N4	91.2(2)	O1−Ni1−N1	87.5(2)
O2−Zn1−N2	85.5(2)	N1−Zn1−N5	108.8(4)	O2−Mn1−N4	82.3(2)	N1−Mn1−N5	112.0(2)	O1−Ni1−N2	177.1(2)
N1−Zn1−N2	92.6(2)	N3−Zn1−N5	106.2(4)	N1−Mn1−N4	89.4(2)	N4−Mn1−N5	105.7(2)	O3−Ni1−O4	85.8(1)
Cl4−Zn2−O1	103.4(1)	O1−Zn2−O2	76.2(3)	Cl2−Mn2−O1	105.7(1)	O1−Mn2−O2	76.2(2)	O3−Ni1−N1	94.6(1)
Cl4−Zn2−O2	105.1(1)	O1−Zn2−N2	89.9(3)	Cl2−Mn2−O2	118.71(1)	O1−Mn2−N2	85.9(2)	O3−Ni1−N2	92.7(2)
Cl4−Zn2−N3	112.7(1)	O1−Zn2−N4	145.1(4)	Cl2−Mn2−N2	100.9(2)	O1−Mn2−N3	138.9(2)	O4−Ni1−N1	178.1(2)
Cl4−Zn2−N4	109.1(1)	O1−Zn2−N6	101.5(4)	Cl2−Mn2−N3	117.0(2)	O1−Mn2−N6	105.3(2)	O4−Ni1−N2	92.3(2)
O1−Zn2−O2	74.0(1)	O2−Zn2−N2	149.6(4)	O1−Mn2−O2	75.1(2)	O2−Mn2−N2	143.6(2)	N1−Ni1−N2	89.6(2)
O1−Zn2−N3	142.2(1)	O2−Zn2−N4	84.7(3)	O1−Mn2−N2	85.2(2)	O2−Mn2−N3	83.6(2)	Cl4−Ni2−O4	79.7(1)
O1−Zn2−N4	88.4(1)	O2−Zn2−N6	105.3(4)	O1−Mn2−N3	137.3(2)	O2−Mn2−N6	110.1(3)	Cl4−Ni2−O5	159.4(1)
O2−Zn2−N3	85.8(1)	N2−Zn2−N4	92.3(4)	O2−Mn2−N2	139.1(2)	N2−Mn2−N3	89.9(2)	Cl4−Ni2−O6	78.0(1)
O2−Zn2−N4	144.4(1)	N2−Zn2−N6	103.9(5)	O2−Mn2−N3	83.2(2)	N2−Mn2−N6	105.1(3)	Cl4−Ni2−N3	103.5(1)
N3−Zn2−N4	90.2(2)	N4−Zn2−N6	111.7(5)	N2−Mn2−N3	88.0(2)	N3−Mn2−N6	115.3(3)	Cl4−Ni2−N4	98.0(1)
				Cl5−Mn3−N8	110.5(2)			O4−Ni2−O5	89.8(2)
				O3−Mn3−O4	74.9(2)			O4−Ni2−O6	91.8(2)
				O3−Mn3−N5	85.5(2)			O4−Ni2−N3	87.9(1)
				O3−Mn3−N8	139.4(2)			O4−Ni2−N4	176.6(1)
				Cl5−Mn3−O3	108.3(1)			O5−Ni2−O6	84.8(2)
				Cl5−Mn3−O4	107.8(1)			O5−Ni2−N3	93.6(2)
				Cl5−Mn3−N5	114.8(2)			O5−Ni2−N4	93.2(2)
				N5−Mn3−N8	89.0(2)			O6−Ni2−N3	178.4(2)
				O4−Mn3−N5	136.8(2)			O6−Ni2−N4	90.2(2)
				O4−Mn3−N8	82.2(2)			N3−Ni2−N4	90.2(2)
				Cl6−Mn4−O4	110.2(1)			Cl4−Ni3−O1	80.8(1)
				Cl6−Mn4−N6	109.0(2)			Cl4−Ni3−O2	161.2(1)
				Cl6−Mn4−N7	115.3(2)			Cl4−Ni3−O6	80.5(1)
				O3−Mn4−O4	75.5(2)			Cl4−Ni3−N5	106.0(2)
				Cl6−Mn4−O3	104.9(1)			Cl4−Ni3−N6	94.9(1)
				O4−Mn4−N7	84.2(2)			O1−Ni3−O2	84.1(2)
				N6−Mn4−N7	88.7(2)			O1−Ni3−O6	93.4(2)
				O3−Mn4−N7	139.3(2)			O1−Ni3−N5	173.2(2)
				O4−Mn4−N6	139.4(2)			O1−Ni3−N6	87.9(2)
				O3−Mn4−N6	84.7(2)			O2−Ni3−O6	89.4(2)
								O2−Ni3−N5	89.5(2)
								O2−Ni3−N6	95.6(2)
								O6−Ni3−N5	88.8(2)
								O6−Ni3−N6	174.9(2)
								N5−Ni3−N6	90.4(2)

[a] Symmetric codes: a, 2 − *x*, 1 − *y*, 1 − *z*; b, 2 − *x*, 2 − *y*, −*z*; c, 1 − *x*, 1 − *y*, −*z*.

Supporting Information), the CH_3-substituted dinuclear cadmium(II) complexes **1** and **5** give negative cotton effects, with two CD peaks corresponding to the UV−vis absorptions at 269 and 397 nm and at 255 and 397 nm (Table 3). In contrast, the Cl-substituted dinuclear cadmium(II) complex **2** shows negative cotton effects, but it has three CD peaks that are consistent with those in the UV−vis spectrum of **2**. The Cl-substituted dinuclear zinc(II) complex **7** also gives negative cotton effects but with two CD peaks corresponding to its UV−vis absorption at 266 and 393 nm. However, the Cl-substituted dinuclear manganese(II) complex **9** indicates positive cotton effects, with two CD peaks corresponding to the UV−vis absorption at 342 and 433 nm, while the Cl-substituted dinuclear manganese(II) complex **10** exhibits one positive cotton effect and one negative cotton effect with CD peaks at 261 and 433 nm.

The fluorescence emission spectra of [3 + 3] macrocyclic ligands **II** and **III** and dinuclear cadmium(II) complexes **1**−**6** are shown in Figure SI3 in the Supporting Information. They all emit strong fluorescence because of their rigid and planar molecular structures, which is a

Scheme 2. Schematic Illustration for the Preparation of Transition-Metal Complexes **1**−**6** (a) and **7**−**12** (b) with Labeling of the Absolute Configuration for the Chiral Carbon Atoms in the Ligands[a]

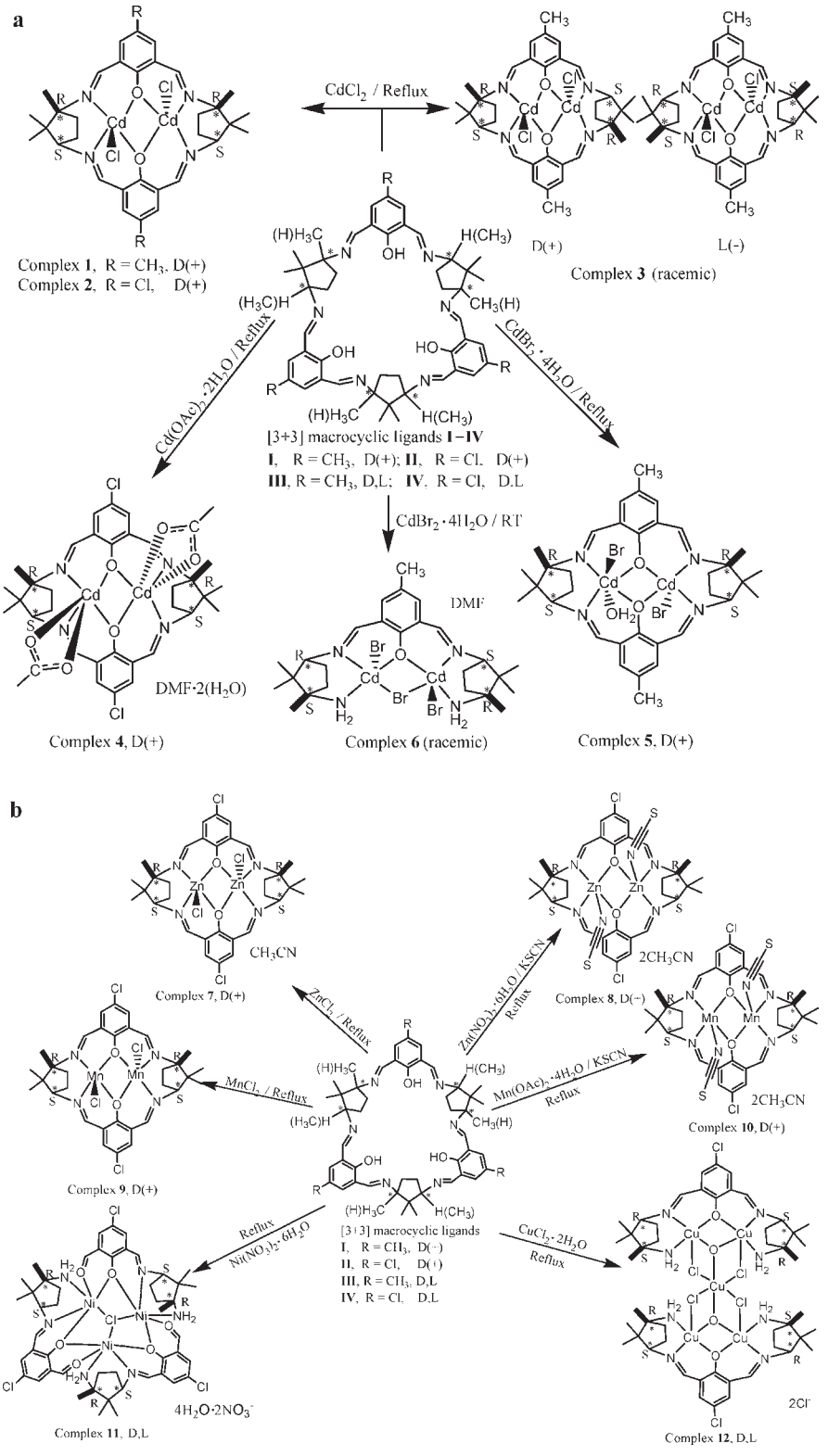

[a] Methyl groups bonded with the chiral carbon atoms are shown in boldface font.

common character for the Robson-type macrocyclic compounds having d^{10} transition-metal centers.[28] The maximum excitation and emission bands of macrocycle ligand **II** are located at 467 and 524 nm, whereas those of ligand **III** are located at 485 and 520 nm. Compared with the ligands, the emission bands of the cadmium(II) complexes are blue-shifted by ca. 21−88 nm.

(28) Dutta, B.; Bag, P.; Flo1rke, U.; Nag, K. *Inorg. Chem.* **2005**, *44*, 147–157.

Table 3. UV−vis, CD, and Fluorescence Absorption Peaks (nm) for Transition-Metal Complexes **1**−**12** and Macrocyclic Schiff-Base Ligands **I**−**IV** at Room Temperature in Methanol

		1	**2**	**3**	**4**	**5**	**6**	**7**	**8**	**9**	**10**	**11**	**12**	**I**	**II**	**III**	**IV**
UV−vis	peak 1	251	202	251	202	258	257	202	202	202	202	202	202	251	202	251	202
	peak 2	372	363	369	329	386	385	248	223	340	382	360	358	373	341	373	341
	peak 3		433		440			370	364	431					442		442
CD	peak 1	269(−)	273(−)			255(−)		266(−)		342(+)	261(−)						
	peak 2	397(−)	392(−)			397(−)		393(−)		433(+)	433(+)						
	peak 3		442(−)														
fluorescence	excitation	397	380	390	432	422	422								467	485	
	emission	439	434	436	476	499	492								524	520	

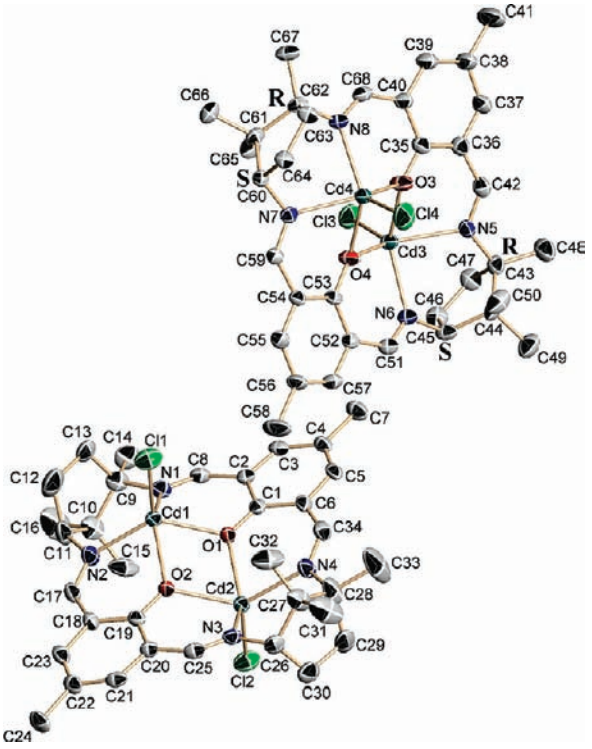

Figure 2. ORTEP diagram (30% thermal probability level ellipsoids) of the molecular structure of [2 + 2] enantiopure dinuclear cadmium(II) complex **1** with the atom-numbering scheme. Hydrogen atoms are omitted for clarity.

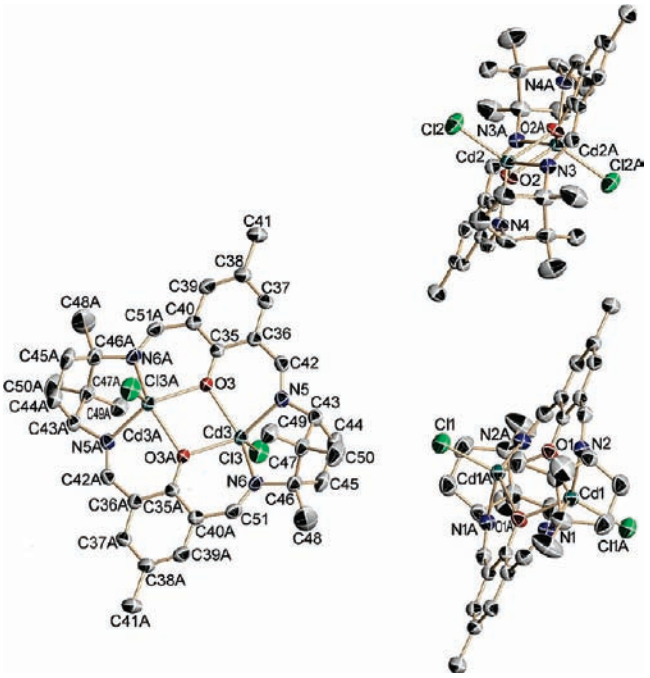

Figure 3. ORTEP diagram (30% thermal probability level ellipsoids) of the molecular structure of [2 + 2] racemic dinuclear cadmium(II) complex **3** with the atom-numbering scheme. Hydrogen atoms and solvent DMF molecules are omitted for clarity.

The ^{1}H NMR spectra of dinuclear cadmium(II) and zinc(II) complexes **1**−**8** exhibit different signals when enantiopure or racemic ligands are present. Namely, the chemical shifts of azomethine, phenyl, and camphoric methine protons in the chiral macrocyclic compounds can be distinguished by splitting into doublets, quartets, or even triplets arising most likely from the second-order coupling effects, while those in the racemic macrocyclic compounds show single peaks (Figures 3 and SI4 in the Supporting Information). The corresponding chemical shifts in CH_3-substituted chiral complex **1** are 8.20 and 8.01 ppm, 7.11 and 7.08 ppm, and 3.55 and 3.54 ppm, while those in Cl-substituted chiral complex **2** are 8.24 and 7.99 ppm, 7.34 and 7.26 ppm, and 3.60, 3.59, and 3.58 ppm. In contrast, racemic complex **3** in the DMSO-d_6 solvent only shows single peaks at 8.34, 7.29, and 3.70 ppm. Furthermore, the two-dimensional ^{1}H−^{1}H COrrelation SpectroscopY (COSY) NMR spectrum of **1** demonstrates the correlations between the methylene protons of a five-membered camphoric carbon ring in the range of 2.1−2.7 ppm, from which the methyl group in the chiral ligand can be easily distinguished by a single peak with a chemical shift of 2.26 ppm.

Similarly, chemical shifts for the azomethine, phenyl, and camphoric methine protons in the chiral dinuclear macrocyclic cadmium(II) complexes **4** and **5** exhibit two groups of peaks in the range of 8.48−8.29, 7.90−7.33, and 3.70−3.68 ppm, while those in the chiral dinuclear macrocyclic zinc(II) complexes **7** and **8** are shifted to a higher field in the range of 8.26−7.99, 7.40−7.28, and 3.61−3.58 ppm by contrast, indicative of the influence of molecular conformation on the chemical shifts.

3.3. Crystal Structures of Dinuclear Macrocyclic Cadmium(II) Complexes 1−3. The molecule structure of **1** with the atom-numbering scheme is shown in Figure 2. Single-crystal X-ray structural studies indicate that **2** has unit cell parameters very similar to those of **1** and only different phenolic substituent groups are found in their molecular structures (CH_3 in **1** versus Cl in **2**). There are two [2 + 2] crystallographically independent macrocyclic dinuclear cadmium(II) molecules in the asymmetric unit cells of **1** and **2** with the absence of any counterions and solvent molecules, and the absolute configuration of eight chiral carbon atoms of camphor diamine units (1*R*,3*S*) is

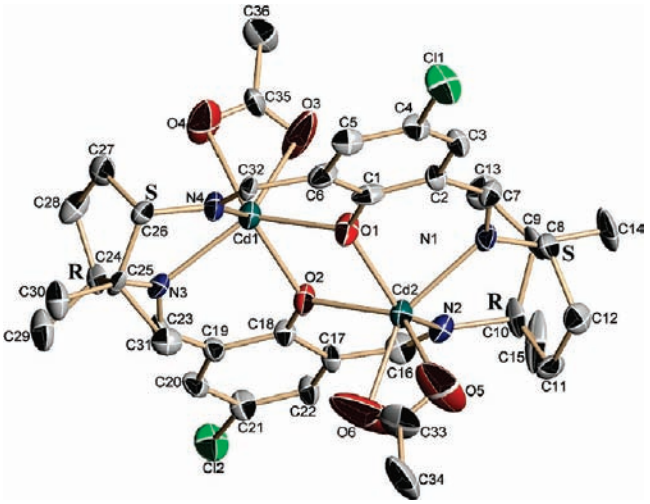

Figure 4. ORTEP diagram (30% thermal probability level ellipsoids) of the molecular structure of [2 + 2] enantiopure dinuclear cadmium(II) complex **4** with the atom-numbering scheme. The absolute configuration of the chiral carbon atoms in the macrocyclic ligand is marked, and the hydrogen atoms and solvent DMF and water molecules are omitted for clarity.

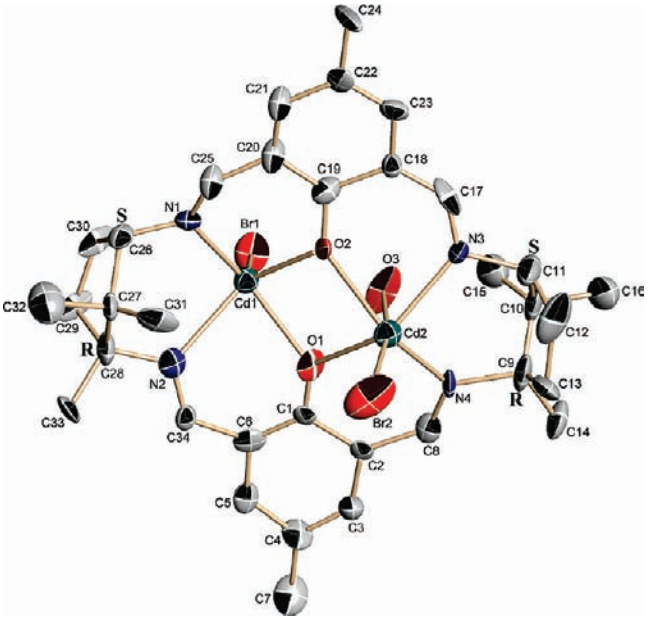

Figure 5. ORTEP drawing of [2 + 2] enantiopure dinuclear cadmium(II) complex **5** showing 30% probability level ellipsoids. The absolute configuration of the chiral carbon atoms in the macrocyclic ligand is marked, and hydrogen atoms are omitted for clarity.

in agreement with those of the starting materials. Reasonable Flack parameters of −0.04(2) in **1** and −0.06(7) in **2** demonstrate the right specification of chirality.[29] In contrast, complex **3** crystallizes in the centrosymmetric triclinic $P\bar{1}$ space group because of the use of a racemic ligand, and there are three halves of [2 + 2] dinuclear cadmium(II) molecules and two free DMF molecules in the asymmetric unit cell, as illustrated in Figure 5.

In complexes **1**−**3**, all of the central cadmium(II) ions adopt the distorted pyramidal geometry where two imino nitrogen atoms and two μ_2-bridging phenol oxygen atoms constitute the basal coordination plane and the apical position is occupied by one Cl^- anion. The two Cl^- counterions from two cadmium(II) centers are located at each side of the dinuclear macrocyclic skeleton to reduce the steric hindrance. Different from our previously studied first-row transition-metal [2 + 2] macrocyclic complexes involving 1,3-propanediamine and *trans*-cyclohexane-1,2-diamine units,[17a,19] where the separation between two metal centers is around 3.2 Å, the radius of the cadmium(II) ion is too larger for the [2 + 2] macrocyclic ligands in **1**−**3** and the planarity of whole macrocyclic complexes cannot be retained. Instead, the two cadmium(II) ions lie above and below the [2 + 2] macrocyclic plane to different extents (Table SI1 in the Supporting Information) in order to minimize the macrocyclic tension. The separations between two cadmium(II) ions are in the range of 3.573(14)−3.612(4) Å in complexes **1**−**3**. It is also noted that the Cd−N bond lengths for the nitrogen atoms bonded to the chiral quaternary carbon atoms are longer than those bonded to the chiral tertiary carbon atoms.

It is worth pointing out that the four chiral carbon atoms in complexes **1**−**3** are arranged in different ways for the enantiopure and racemic [2 + 2] macrocyclic ligands. Namely, for the enantiopure macrocyclic ligands in **1** and **2**, the arrangement of four chiral carbon atoms is *RRSS*, where the two methyl groups bonded to the chiral carbon atoms occupy the adjacent vertices of a chiral carbon atom parallelogram. Nevertheless, for the racemic macrocyclic ligand in complex **3**, equal amounts of chiral [2 + 2] macrocyclic skeletons are present, bearing two 1*R*,3*S* and two 1*S*,3*R* camphoric diamine units, respectively. That is to say, 1*R*,3*S* and 1*S*,3*R* camphoric diamine units are not involved in one [2 + 2] macrocyclic ligand. Thus, two new types of *RSRS* arrangements are formed where the two methyl groups bonded to the chiral carbon atoms occupy the diagonal positions of the chiral carbon atom parallelogram.

Complexes **1** and **2** have different crystal structures from **3** because of the presence of different macrocyclic ligands (enantiopure and racemic) and solvent molecules (with or without DMF). Effective $\pi-\pi$ stacking interactions can be observed between the neighboring aromatic rings only in the crystal packing of **3** with the centroid−centroid separation of 3.590 Å (Figure SI5 in the Supporting Information).

3.4. Crystal Structures of Dinuclear Cadmium(II) Complexes 4−**6.** Single-crystal X-ray diffraction studies on **4** indicate that the asymmetric unit of **4** contains one [2 + 2] dinuclear cadmium(II) complex and one DMF and two water molecules. The molecular structure of **4** with the atom-numbering scheme is shown in Figure 4, where each cadmium(II) center exhibits coordination geometry similar to that of **1**−**3** except that the apical position for each is occupied by two oxygen atoms of the acetate anion, with the Cd−O bond lengths in the range of 2.253(10)−2.314(13) Å and a distance of Cd1···Cd2 of 3.617(11) Å. The two acetate anions adopt the trans configuration relative to the macrocyclic plane with a dihedral angle of 47.8(4)°. The arrangement of four chiral carbon atoms in **4** is *RRSS* because of the use of an enantiopure ligand similar to that in **1** and **2**.

The molecular structures of **5** and **6** with the atom-numbering scheme are illustrated in Figures 5 and 6,

(29) Flack, H. D. *Acta Crystallogr.* **1983**, *A39*, 876–881.

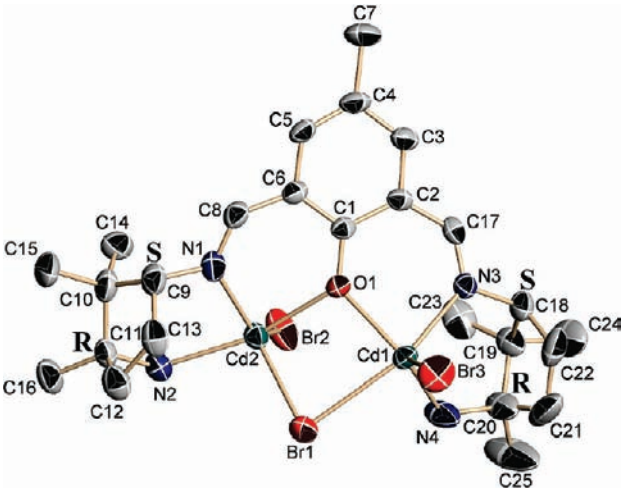

Figure 6. ORTEP drawing of racemic dinuclear cadmium(II) complex **6** showing 30% probability level ellipsoids. The absolute configuration of the chiral carbon atoms in the acyclic ligand is marked, and hydrogen atoms are omitted for clarity.

respectively. They crystallize in the monoclinic chiral $P2_1$ (**5**) and centrosymmetric $C2/c$ (**6**) space groups because of the use of enantiopure and racemic ligands. **5** is a [2 + 2] macrocyclic dinuclear cadmium(II) complex with a Cd1···Cd2 distance of 3.603(12) Å, while **6** is a [1 + 2] acyclic dinuclear cadmium(II) complex with a longer Cd1···Cd2 distance of 3.621(8) Å. The two cadmium(II) centers in **5** adopt different coordination geometries, where Cd1 is five-coordinated, exhibiting a distorted tetragonal pyramid, and Cd2 is six-coordinated, adopting a distorted octahedron. Besides the two imino nitrogen atoms and the two phenolic oxygen atoms in the equatorial plane, the apical position of the pyramid for Cd1 is occupied by a Br^- ion and the two axial positions of the octahedron for Cd2 are occupied by a Br^- ion and a water molecule. With regard to complex **6**, each five-coordinate cadmium(II) center adopts a distorted tetragonal-pyramidal geometry where one imine nitrogen atom, one phenolic oxygen atom, one amine group of the camphoric diamine unit, and one μ_2-bridging Br^- anion form the equatorial plane and another terminal Br^- anion occupies the apical position at each side of the macrocyclic plane.

It is noted that complex **6** is a ring-degradation intermediate from the Schiff-base macrocyclic ligands. Because of the different steric hindrance effects for the two chiral carbon atoms (with or without the methyl group) and the use of a racemic macrocyclic ligand, the amine group in the camphoric diamine unit linked to the chiral carbon atom with larger steric hindrance is preferentially formed in the ring-degradation process and equal amounts of D-(+)- and L-(−)-camphoric fragments are present in **6**. No effective $\pi-\pi$ stacking interactions can be found in the crystal packing of **4**−**6**.

3.5. Crystal Structures of Dinuclear Macrocyclic Zinc(II) and Manganese(II) Complexes 7−10. The molecule structures of [2 + 2] dinuclear zinc(II) complexes **7** and **8** with the atom-numbering scheme are illustrated in Figures 7 and 8, respectively. The asymmetric unit of **7** contains one dinuclear zinc(II) complex and one solvent acetonitrile molecule, while **8** is composed of one dinuclear zinc(II) complex and two solvent acetonitrile molecules. Each zinc(II) center in **7** and **8** exhibits a distorted five-coordinate pyramidal configuration, where two imino nitrogen atoms and two μ_2-bridging phenol oxygen atoms constitute the basal coordination plane and the axial position is occupied by one Cl^- anion in **7** and one N-coordinated SCN^- anion in **8** at each side of the macrocyclic plane. In comparison with the ligand conformation in dinuclear cadmium(II) complexes, an analogous arrangement of four chiral carbon atoms in **7** and **8** is observed (both in the *RRSS* configuration), corresponding

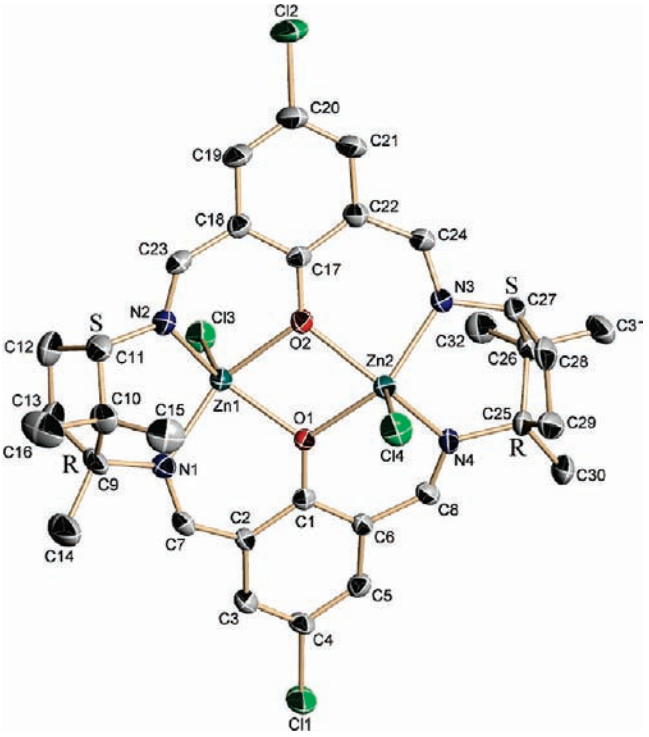

Figure 7. ORTEP drawing of enantiopure dinuclear zinc(II) complex **7** showing 30% probability level ellipsoids. The absolute configuration of the chiral carbon atoms in the macrocyclic ligand is marked, and hydrogen atoms and solvent CH_3CN molecules are omitted for clarity.

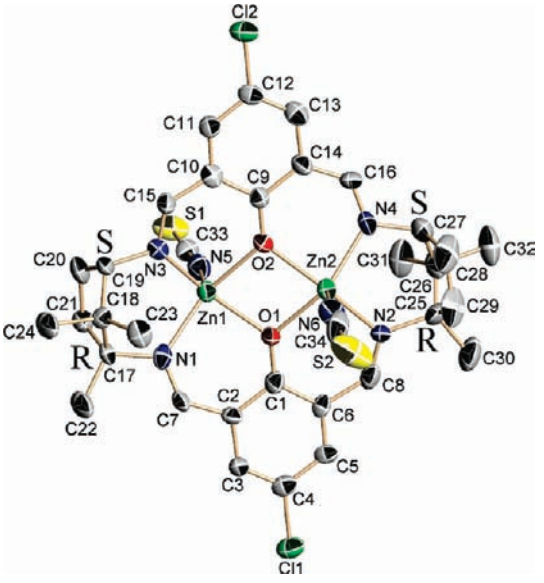

Figure 8. ORTEP drawing of enantiopure dinuclear zinc(II) complex **8** showing 30% probability level ellipsoids. The absolute configuration of the chiral carbon atoms in the macrocyclic ligand is marked, and hydrogen atoms and solvent CH_3CN molecules are omitted for clarity.

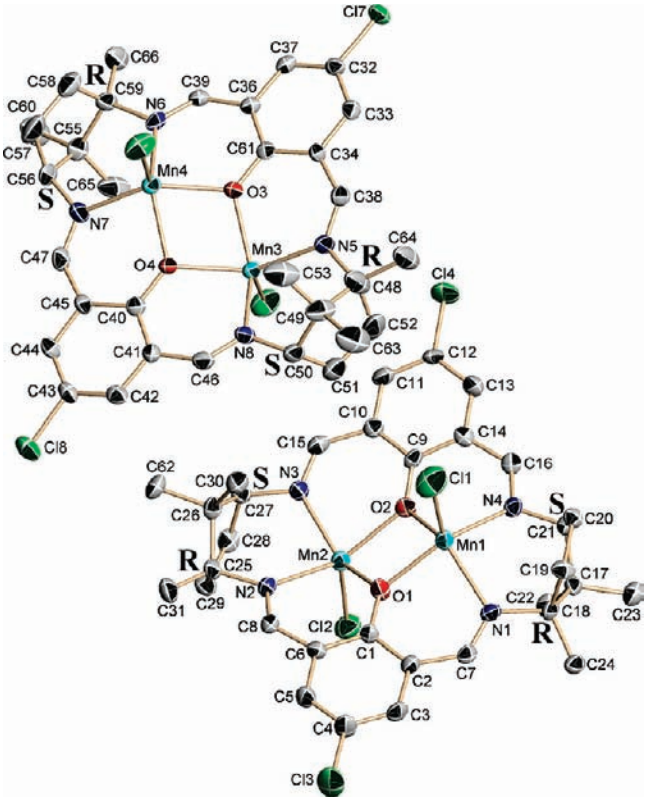

Figure 9. ORTEP drawing of enantiopure dinuclear manganese(II) complex **9** showing 30% probability level ellipsoids. The absolute configuration of the chiral carbon atoms in the macrocyclic ligand is marked, and hydrogen atoms are omitted for clarity.

to the use of a chiral ligand. However, the size effects of different d^{10} metal ions on the macrocyclic conformation have been shown because the planarity of dinuclear zinc(II) complexes is obviously better than that of dinuclear cadmium(II) complexes **1**−**6**. The mean deviations from the coordination plane and the distances between the least-squares plane and the center metal in **7** and **8** are shortened because of the smaller radius of the zinc(II) ion (Table SI1 in the Supporting Information). Additionally, the Zn1···Zn2 separations in **7** and **8** are 3.314(4) and 3.269(7) Å, respectively, which are significantly shorter than those in dinuclear cadmium(II) complexes **1**−**6**.

The molecular structures of [2 + 2] dinuclear manganese(II) complexes **9** and **10** with the atom-numbering scheme are illustrated in Figures 9 and 10, respectively. The asymmetric unit of **9** contains two dinuclear manganese(II) complexes, whereas the asymmetric unit of **10** contains one dinuclear manganese(II) complex and two solvent acetonitrile molecules. Similarly, the manganese(II) centers in **9** and **10** exhibit a distorted five-coordinate pyramidal geometry, where two imino nitrogen atoms and two μ_2-bridging phenol oxygen atoms constitute the basal plane. The apical position is occupied by one Cl^- anion in **9** and one N-coordinated SCN^- anion in **10** at each side of the macrocyclic plane. The ligand conformation is also in the *RRSS* arrangement, corresponding to the use of a chiral macrocyclic ligand. The separations between the two manganese(II) centers are 3.358(2) and 3.366(2) Å in **9** and 3.325(2) Å in **10**, respectively, which are somewhat larger than those between the two zinc(II)

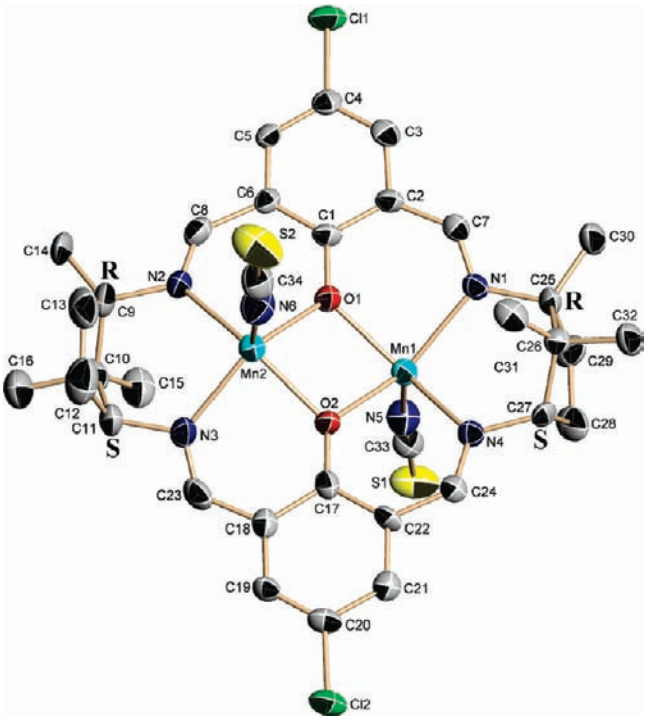

Figure 10. ORTEP drawing of enantiopure dinuclear manganese(II) complex **10** showing 30% probability level ellipsoids. The absolute configuration of the chiral carbon atoms in the macrocyclic ligand is marked, and hydrogen atoms and solvent CH_3CN molecules are omitted for clarity.

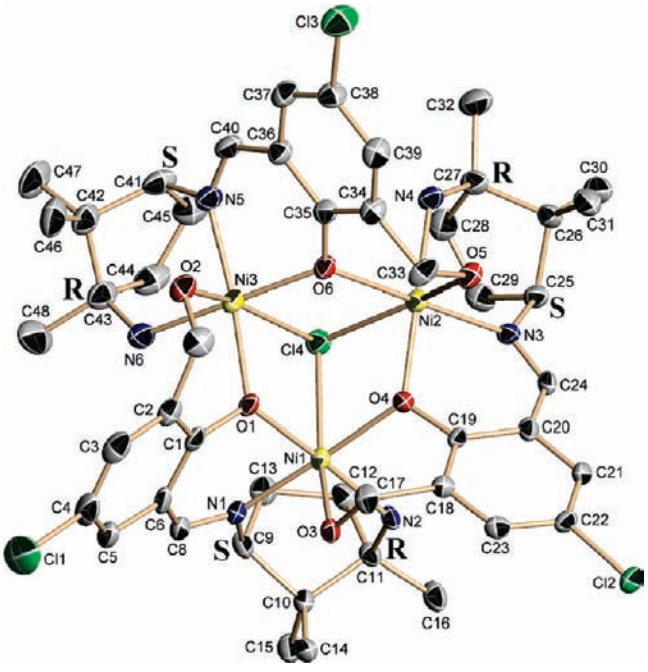

Figure 11. ORTEP drawing of the cationic structure of [1 + 1] trinuclear nickel(II) complex **11** showing 30% probability level ellipsoids. The absolute configuration of the chiral carbon atoms in the acyclic ligand is marked, and hydrogen atoms, solvent water molecules, and NO_3^- anions are omitted for clarity.

centers in **7** and **8** mainly arising from the larger radius of the manganese(II) ion.

3.6. Crystal Structures of Trinuclear Nickel(II) and Pentanuclear Copper(II) Complexes 11 and 12. The cationic structures of **11** and **12** with the atom-numbering

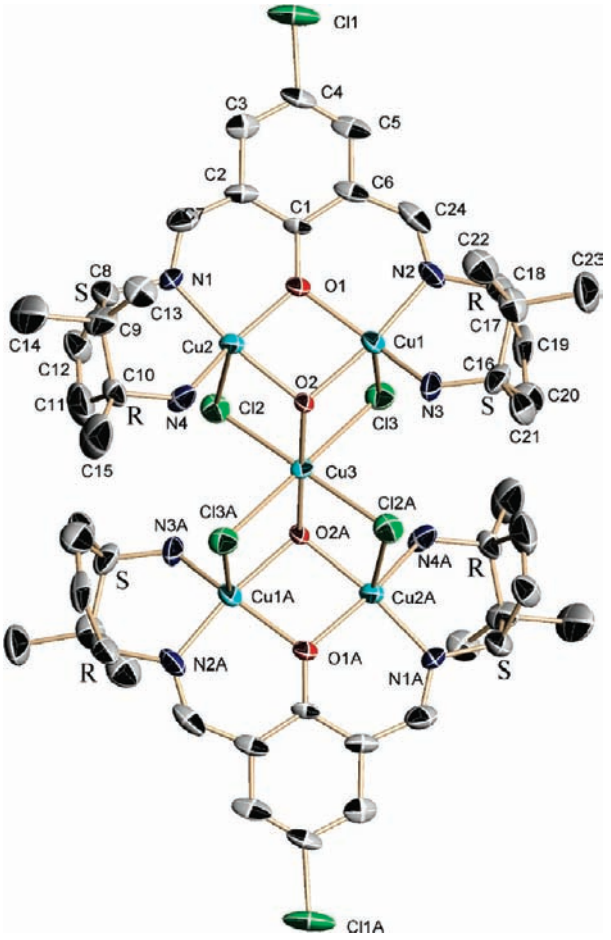

Figure 12. ORTEP drawing of the cationic structure of [1 + 2] pentanuclear copper(II) complex **12** showing 30% probability level ellipsoids. The absolute configuration of the chiral carbon atoms in the acyclic ligand is marked, and hydrogen atoms, anions, and solvent molecules are omitted for clarity.

scheme are illustrated in Figures 11 and 12, respectively. Single-crystal X-ray diffraction studies on **11** reveal that the asymmetric unit contains one trinuclear [1 + 1] acyclic nickel(II) divalent cation, two NO_3^- anions, and four water molecules. Three six-coordinate nickel(II) centers in **11** exhibit an elongated octahedronal geometry, where each nickel(II) ion is coordinated by two nitrogen atoms belonging to one camphoric diamine unit, two μ_2-phenol oxygen atoms belonging to different phenylic rings, one oxygen atom belonging to the aldehyde group, and one μ_3-Cl atom (Cl4). The distances between the neighboring nickel(II) centers are 3.470(5) (Ni1···Ni2), 3.403(5) (Ni1···Ni3), and 3.442(5) Å (Ni2···Ni3), respectively.

The divalent cation of **12** contains four five-coordinate and one six-coordinate copper(II) centers countered by four μ_2-Cl, two μ_3-OH bridges, and two μ_2-bridging phenol oxygen atoms. The corresponding Cu···Cu separations in **12** are 3.073(2) (Cu1···Cu2 in the macrocyclic plane), 3.249(2) (Cu1···Cu3), and 3.310(2) Å (Cu2···Cu3). It is also noted that the arrangement of the chiral carbon atoms in trinuclear nickel(II) and pentanuclear copper(II) complexes **11** and **12** (*RSRS*) is in well agreement with that in dinuclear cadmium(II) complexes having racemic ligands (**3** and **6**). Moreover, the degradation of macrocyclic ligands in **11** and **12** preferentially takes place at the chiral carbon atoms of camphoric diamine

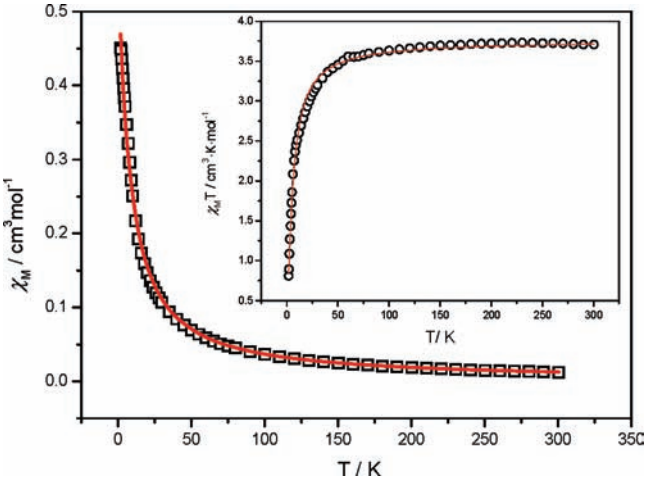

Figure 13. Temperature dependence of the magnetic susceptibility of **11** on the forms of $\chi_M T$ and $\chi_M T$ vs T plots. The open boxes and open circles (the inset) are the experimental data, and the red solid lines are the best-fitting curves.

units bearing the methyl group because of their stronger spatial crowding effects than the ones bearing the hydrogen atom, which is the same as that in the acyclic [1 + 2] dinuclear cadmium(II) complex **6**.

3.7. Magnetic Study for Trinuclear Nickel(II) Complex 11. The variable-temperature (1.8−300 K) magnetic susceptibility of **11** was measured on a SQUID magnetometer at an applied field of 2 kOe, and the χ_M and $\chi_M T$ versus T plots are shown in Figure 13. The $\chi_M T$ value is 3.71 cm^3 K mol^{-1} [based on three nickel(II) ions] at 300 K (the inset in Figure 13), and it reaches 0.89 cm^3 K mol^{-1} at 1.8 K. The high-temperature $\chi_M T$ values correspond to the theoretical spin-only value expected for three uncoupled nickel(II) ions with $S = 1$, and the gradual decrease of the $\chi_M T$ values observed upon cooling indicates an antiferromagnetic coupling between the nickel(II) ions mediated by the μ_3-Cl and μ_2-OH bridges in **11**.

For symmetry reasons, the Ni_3 triangular unit in **11** can be regarded as an equilateral triangle with three equal pairwise magnetic interactions. The corresponding isotropic spin Hamiltonian H is given in eq 1,[30] and the best parameters obtained by a standard least-squares-fitting program (eq 2) are $g = 2.24(1)$ and $J = -1.06(2)$ cm^{-1} with $R = 0.995$. These values are comparable with those of another similar trinuclear nickel(II) unit in the literature exhibiting antiferromagnetic coupling interactions.[31]

$$\hat{H} = -2J(\hat{S}_1\hat{S}_2 + \hat{S}_2\hat{S}_3 + \hat{S}_3\hat{S}_1) \qquad (1)$$

$$\chi_M = \frac{Ng^2\beta^2}{3kT} \times \frac{6e^{2J/kT} + 6e^{2J/kT} + 30e^{6J/kT} + 6e^{2J/kT} + 30e^{6J/kT} + 84e^{12J/kT}}{3e^{2J/kT} + 1 + 3e^{2J/kT} + 5e^{6J/kT} + 3e^{2J/kT} + 5e^{6J/kT} + 7e^{12J/kT}}$$

$$= \frac{2Ng^2\beta^2}{kT} \frac{3e^{2J/kT} + 10e^{6J/kT} + 14e^{12J/kT}}{1 + 9e^{2J/kT} + 10e^{6J/kT} + 7e^{12J/kT}} \qquad (2)$$

(30) Kahn, O. *Molecular Magnetism*; VCH-Wiley: Weinheim, Germany, 1993.
(31) Spielberg, E. T.; Görls, H.; Plass, W. *Inorg. Chim. Acta* **2007**, *360*, 3925–3931.

4. Conclusions

In summary, we have reported the syntheses and structural and spectral characterizations of four novel [3 + 3] enantiopure and racemic macrocycles **I**−**IV** condensed from 2,6-diformyl-4-substituted phenols (R = CH_3 or Cl) and hydrochloride and sulfate salts of D-(+)- and D,L-camphoric diamines via a sodium template method as well as a series of multinuclear cadmium(II), zinc(II), manganese(II), nickel(II), and copper(II) complexes. In the course of metal-ion complexation, cleavage and reorganization of ligands **I**−**IV** take place, forming the corresponding ring-contraction [2 + 2], [1 + 2], and [1 + 1] types of metal complexes. Reorganization of the resulting metal−organic complexes can be attributed to the size effect and restriction of the coordination geometry of the central metals, steric hindrance of ligands, the presence of different counterions, and experimental conditions.

In the formation of acyclic [1 + 1] trinuclear complex **11** and [1 + 2] dinuclear and pentanuclear complexes **6** and **12**, the degradation of macrocyclic ligands preferentially takes place at the chiral carbon atoms of camphoric diamine units bearing the methyl group because of their stronger spatial crowding effects than the ones bearing the hydrogen atom. It is also found that the sequence of separations between the metal centers in dinuclear cadmium(II), zinc(II), and manganese(II) complexes **1**−**10** is well consistent with that of the ionic radii shortened from cadmium(II) to manganese(II) to zinc(II) ions. More interestingly, the use of enantiopure and racemic ligands results in different arrangements of the camphoric diamine units (*RRSS* for the enantiopure ligands in complexes **1**, **2**, **4**, **5**, and **7**−**10** and *RSRS* for the racemic ligands in complexes **3**, **6**, **11**, and **12**), crystal symmetries, and ^{1}H NMR and CD spectra for related compounds. In addition, different substituent groups in the benzene rings of macrocyclic ligands and different counterions used give rise to variations of their electronic spectra.

Acknowledgment. W.H. acknowledges the Major State Basic Research Development Programs (Grants 2007CB-925101 and 2006CB806104), the National Natural Science Foundation of China (Grants 20871065 and 20721002), and the Jiangsu Province Department of Science and Technology (Grant BK2009226) for financial aid.

Supporting Information Available: X-ray crystallographic data in CIF format for **1**−**12**, experimental details, partial ESI-MS and NMR graphs, and a perspective view of the crystal packing of **3**. This material is available free of charge via the Internet at http://pubs.acs.org. CCDC nos. 741965−741970 (**1**−**6**) and 764374−764378 (**7**−**11**) contain the supplementary crystallographic data of the metal complexes. These data can also be obtained free of charge, upon request, at www.ccdc.cam.ac.uk/conts/retrieving.html [or from the Cambridge Crystallographic Data Centre, 12 Union Road, Cambridge CB2 1EZ, U.K.; fax (internet) +44-1223/336-033; e-mail deposit@ccdc.cam.ac.uk].